

Review

A Review of Magnetic Flux Leakage Nondestructive Testing

Bo Feng ¹, Jianbo Wu ^{2,*}, Hongming Tu ², Jian Tang ¹ and Yihua Kang ¹

¹ School of Mechanical Science and Engineering, Huazhong University of Science and Technology, Wuhan 430074, China

² School of Mechanical Engineering, Sichuan University, Chengdu 610065, China

* Correspondence: wujianbo@scu.edu.cn

Abstract: Magnetic flux leakage (MFL) testing is a widely used nondestructive testing (NDT) method for the inspection of ferromagnetic materials. This review paper presents the basic principles of MFL testing and summarizes the recent advances in MFL. An analytical expression for the leakage magnetic field based on the 3D magnetic dipole model is provided. Based on the model, the effects of defect size, defect orientation, and liftoff distance have been analyzed. Other influencing factors, such as magnetization strength, testing speed, surface roughness, and stress, have also been introduced. As the most important steps of MFL, the excitation method (a permanent magnet, DC, AC, pulsed) and sensing methods (Hall element, GMR, TMR, etc.), have been introduced in detail. Finally, the algorithms for the quantification of defects and the applications of MFL have been introduced.

Keywords: MFL; NDT; sensor; magnetic dipole model; high speed; liftoff; magnetizer; inverse problem; artificial neural network



Citation: Feng, B.; Wu, J.; Tu, H.; Tang, J.; Kang, Y. A Review of Magnetic Flux Leakage Nondestructive Testing. *Materials* **2022**, *15*, 7362. <https://doi.org/10.3390/ma15207362>

Academic Editor: Danny V. van Hemelrijck

Received: 26 September 2022

Accepted: 12 October 2022

Published: 20 October 2022

Publisher's Note: MDPI stays neutral with regard to jurisdictional claims in published maps and institutional affiliations.



Copyright: © 2022 by the authors. Licensee MDPI, Basel, Switzerland. This article is an open access article distributed under the terms and conditions of the Creative Commons Attribution (CC BY) license (<https://creativecommons.org/licenses/by/4.0/>).

1. Introduction

Magnetic flux leakage (MFL) testing is an electromagnetic nondestructive testing (NDT) method with high efficiency and reliability. It has the ability to detect various types of defects such as cracks, corrosion, pitting, and cavity, and it is able to detect both surface and subsurface defects. Therefore, it has been widely used to ensure the integrity and safety of structures in the petrochemical, energy, manufacturing, and transportation industries.

The principle of MFL testing is based on the interaction between magnetic field and defects. The MFL testing device usually consists of a magnetizing unit, a sensing unit, a signal conditioning unit, an analog-to-digital converter (ADC), and a computer with signal displaying and analyzing software. The magnetizing unit is usually consisting of permanent magnets of magnetizing coils that are able to magnetize the ferromagnetic specimen into saturation or near saturation. Due to the abrupt change in magnetic reluctance at the defects, the magnetic flux leaks into the nearby air. The perturbation of the magnetic field can be recorded by an array of magnetic field sensors and used to evaluate and quantify defects.

MFL testing theory and technology have been developed for decades. There are several review papers that summarized some developments in MFL together with other electromagnetic NDT methods [1–4]. However, there is no comprehensive review of MFL technology. In the following sections of this paper, a comprehensive review will be given to the following subjects of MFL technology: (1) the study of the MFL principle and analytical model; (2) the influence of testing parameters (e.g., magnetizing strength, liftoff, scanning speed) and defect properties (e.g., defect size and defect orientation) on the MFL signals; (3) excitation and sensing techniques in MFL testing; (4) inverse problem and defect quantification in MFL; (5) applications of MFL and comparison with related NDT methods.

2. MFL Principle and Analytical Model

2.1. MFL Principle

The basic principle of MFL testing is schematically shown in Figure 1, where a magnetizer is applied to magnetize the ferromagnetic specimen into near saturation. The

magnetizer can be either a magnet with a ferromagnetic yoke or a magnetizing coil. Due to the high permeability of ferromagnetic materials, the magnetic flux is constrained in the material when no defects are presented. In the presence of a defect, the magnetic field leaks into the nearby air and causes the leakage field.

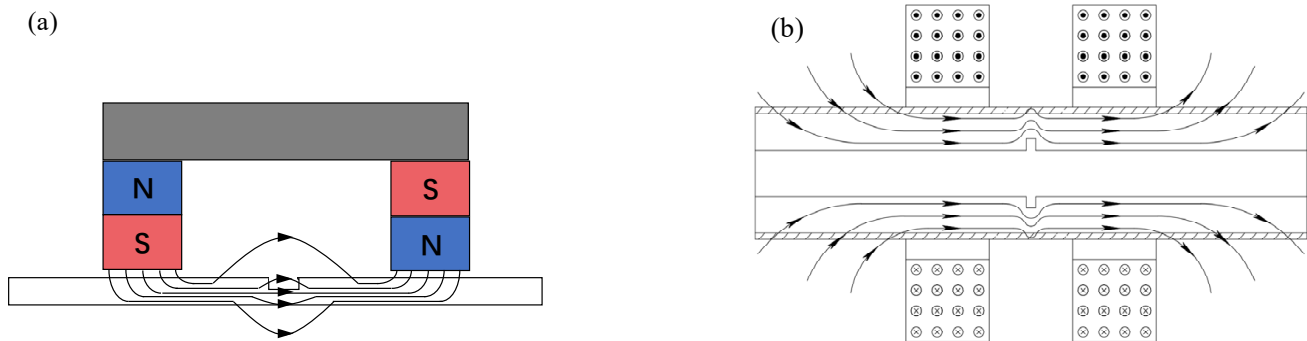


Figure 1. Basic principle of MFL testing: (a) yoke-type magnetizer; (b) encircling coil-type magnetizer.

The phenomenon of magnetic field leakage was explained using the refraction of the magnetic field by Sun and Kang with the boundary conditions of the electromagnetic field [5], as shown in Figure 2a. At the interface of the two media, the magnetic fields satisfy the boundary equations; thus, the refracted angle is expressed as:

$$\alpha_2 = \arctan\left(\frac{\mu_2}{\mu_1} \tan \alpha_1\right) \quad (1)$$

where μ_1 and μ_2 are the permeabilities of medium 1 and 2, respectively.

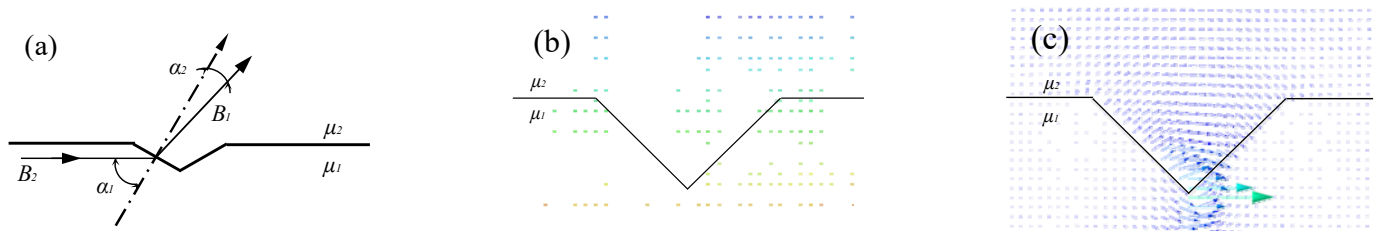


Figure 2. The refraction of magnetic field at interface of a defect: (a) schematic representation; (b) finite element simulation results of magnetic vectors for $\mu_1 = \mu_2$; (c) finite element simulation results of magnetic vectors for $\mu_1 > \mu_2$.

Therefore, if $\mu_1 = \mu_2$, which is the case where the specimen is non-ferromagnetic, then $\alpha_1 = \alpha_2$. In this case, the flux line continues at the interface without any perturbation, and there is no leakage magnetic field. If $\mu_1 > \mu_2$, then $\alpha_1 > \alpha_2$, and the magnetic field will enter the vicinity of the defect due to refraction.

2.2. Forward Problem and Magnetic Dipole Model

The forward problem, which derives the MFL field of a defect with a certain shape, is a fundamental and important topic in MFL testing. One of the most commonly used models in the forward problem is the magnetic dipole model, the study of which was pioneered by Zatsepin and Shcherbinin [6,7]. Based on their study, many researchers have further derived the distribution of the leakage field generated by a 2D notch and a 3D notch [8,9]. The dipole is assumed to distribute uniformly at the slot surfaces with the density σ_m . For a line with infinitesimal length dy on the slot surface shown in Figure 3a, the magnetic charge is $dp = \sigma_m dy$, and in the 3D model shown in Figure 3b, the charge is $dp = \sigma_m dy dz$. The magnetic field generated by the magnetic charge is $d\mathbf{H} = \frac{dp}{4\pi r^3} \mathbf{r}$. By taking the integral for

all magnetic charges at slot surfaces, the magnetic field can be derived. For the 2D model in Figure 3a, the tangential and normal components of the field are:

$$H_x(x, y) = \frac{\sigma_m}{2\pi} \left[\arctan \frac{b(x+a)}{(x+a)^2 + y(y+b)} - \arctan \frac{b(x-a)}{(x-a)^2 + y(y+b)} \right] \quad (2)$$

$$H_y(x, y) = \frac{\sigma_m}{4\pi} \ln \left(\frac{[(x+a)^2 + (y+b)^2][(x-a)^2 + y^2]}{[(x+a)^2 + y^2][(x-a)^2 + (y+b)^2]} \right) \quad (3)$$

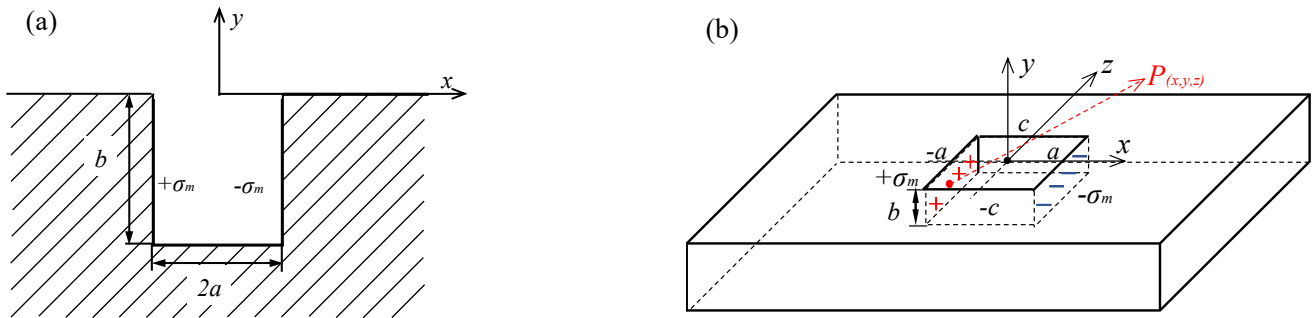


Figure 3. Dipole model for the magnetic field calculation: (a) 2D representation; (b) 3D representation.

For the 3D model in Figure 3b, the results are:

$$\begin{aligned} H_x(x, y, z) = & \frac{\sigma_m}{4\pi} \left(\arctan \frac{(y+b)(z+c)}{(x+a)[(x+a)^2 + (y+b)^2 + (z+c)^2]^{1/2}} - \arctan \frac{y(z+c)}{(x+a)[(x+a)^2 + y^2 + (z+c)^2]^{1/2}} \right. \\ & - \arctan \frac{(y+b)(z-c)}{(x+a)[(x+a)^2 + (y+b)^2 + (z-c)^2]^{1/2}} + \arctan \frac{y(z-c)}{(x+a)[(x+a)^2 + y^2 + (z-c)^2]^{1/2}} \\ & - \arctan \frac{(y+b)(z+c)}{(x-a)[(x-a)^2 + (y+b)^2 + (z+c)^2]^{1/2}} + \arctan \frac{y(z+c)}{(x-a)[(x-a)^2 + y^2 + (z+c)^2]^{1/2}} \\ & \left. + \arctan \frac{y(z-c)}{(x-a)[(x-a)^2 + (y+b)^2 + (z-c)^2]^{1/2}} - \arctan \frac{y-a}{(x-a)[(x-a)^2 + y^2 + (z-c)^2]^{1/2}} \right) \quad (4) \end{aligned}$$

$$\begin{aligned} H_y(x, y, z) = & \frac{\sigma_m}{4\pi} \left[\ln \left(\frac{z+c + [(x+a)^2 + y^2 + (z+c)^2]^{1/2}}{z-c + [(x+a)^2 + y^2 + (z-c)^2]^{1/2}} \right) \times \frac{z-c + [(x+a)^2 + (y+b)^2 + (z-c)^2]^{1/2}}{z+c + [(x+a)^2 + (y+b)^2 + (z+c)^2]^{1/2}} \right. \\ & \left. - \ln \left(\frac{z+c + [(x-a)^2 + y^2 + (z+c)^2]^{1/2}}{z-c + [(x-a)^2 + y^2 + (z-c)^2]^{1/2}} \right) \times \frac{z-c + [(x-a)^2 + (y+b)^2 + (z-c)^2]^{1/2}}{z+c + [(x-a)^2 + (y+b)^2 + (z+c)^2]^{1/2}} \right) \quad (5) \end{aligned}$$

$$\begin{aligned} H_z(x, y, z) = & \frac{\sigma_m}{4\pi} \left[\ln \left(\frac{y+b + [(x+a)^2 + (y+b)^2 + (z-c)^2]^{1/2}}{y + [(x+a)^2 + y^2 + (z-c)^2]^{1/2}} \right) \times \frac{y + [(x+a)^2 + y^2 + (z+c)^2]^{1/2}}{y+b + [(x+a)^2 + (y+b)^2 + (z+c)^2]^{1/2}} \right. \\ & \left. - \ln \left(\frac{y+b + [(x-a)^2 + (y+b)^2 + (z-c)^2]^{1/2}}{y + [(x-a)^2 + y^2 + (z-c)^2]^{1/2}} \right) \times \frac{y + [(x-a)^2 + y^2 + (z+c)^2]^{1/2}}{y+b + [(x-a)^2 + (y+b)^2 + (z+c)^2]^{1/2}} \right) \quad (6) \end{aligned}$$

According to Equations (4)–(6), the distribution of magnetic field above a notch can be calculated. Figure 4 shows the magnetic field distributions at liftoff $y = 1$ for defects with the dimensions of $a = 1, b = 2, c = 10$ and $a = 5, b = 2, c = 5$.

The magnetic dipole model was further extended to calculate the magnetic field generated by defects with various shapes. Uetake studied the MFL of adjacent parallel surface slots [10]. Dutta and Stanley calculated the MFL of a cylindrical hole and verified the model by comparing it with simulation results [11,12]. Mandache and Clapham calculated the MFL of a cylindrical hole, a racetrack defect, and adjacent holes [13]. Lukyanets derived an analytical model for the MFL of a defect with a smooth surface [14]. Trevino proposed an improved dipole model to calculate the MFL of conical, ellipsoidal, and tensional shaped defects [15]. Wu proposed a model for concave and bump shaped defects [16]. Zhang

derived an analytical expression for internal defects using a modified dipole model and image theory [17]. Li proposed to improve the accuracy of the dipole model by considering a two-layer charge distribution model [18].

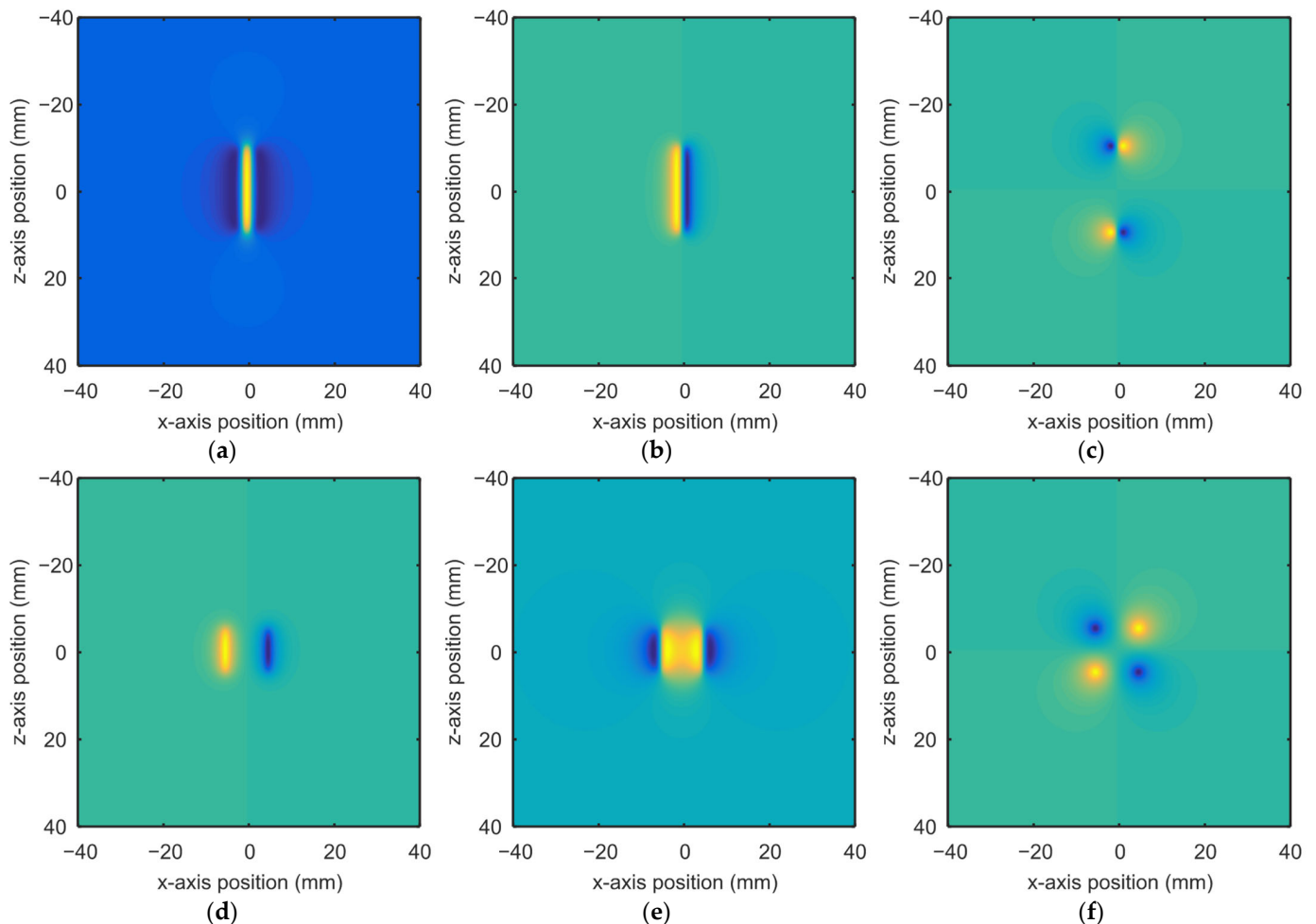


Figure 4. Distribution of magnetic field above defects with colors indicating the intensity of magnetic field: (a) H_x for a rectangular notch; (b) H_y for a rectangular notch; (c) H_z for a rectangular notch; (d) H_x for a square notch; (e) H_y for a square notch; (f) H_z for a square notch.

In addition to the commonly used magnetic dipole model, there are also some analytical models derived for the calculation of the MFL. Bowler derived an analytical solution for semi-elliptical indentation by solving the Laplace equation of a static magnetic field, and the results turned to be in agreement with those from the dipole model [19]. Cheng and Wang proposed a solenoid model based on the magnetization mechanisms of the magnetic medium, and calculated the V-shaped and Z-shaped defects [20,21]. Huang used a basic signal analysis approach to predict the MFL response with high accuracy and calculation speed [22].

3. Factors Influencing MFL Signal

In MFL testing, there are many factors that influence the inspection signal. This section summarizes some of the important factors such as the defect size, defect orientation, lift-off distance, magnetization strength, stress, and scanning velocity.

3.1. Defect Dimension and Orientation

The influence of defect size on the MFL signal has been analyzed using analytical models, simulations, and experiments [8,23–29]. It was suggested by Förster that [8], when

using the magnetic dipole model to analyze the influence of defect dimension, the magnetic charge density should also change with defect dimension to obtain more accurate results:

$$\sigma_m = \frac{1}{2\pi} \frac{b/a + 1}{(1/\mu)b/a + 1} F_{nl} H_a \tag{7}$$

where F_{nl} is a non-linear factor and H_a is the applied field.

The influence of the defect dimensions can be analyzed using Equations (4)–(7). For the defect shown in Figure 3b, the magnetic field above the center of the defect ($y = 1, z = 0$) was extracted and the results are shown in Figure 5.

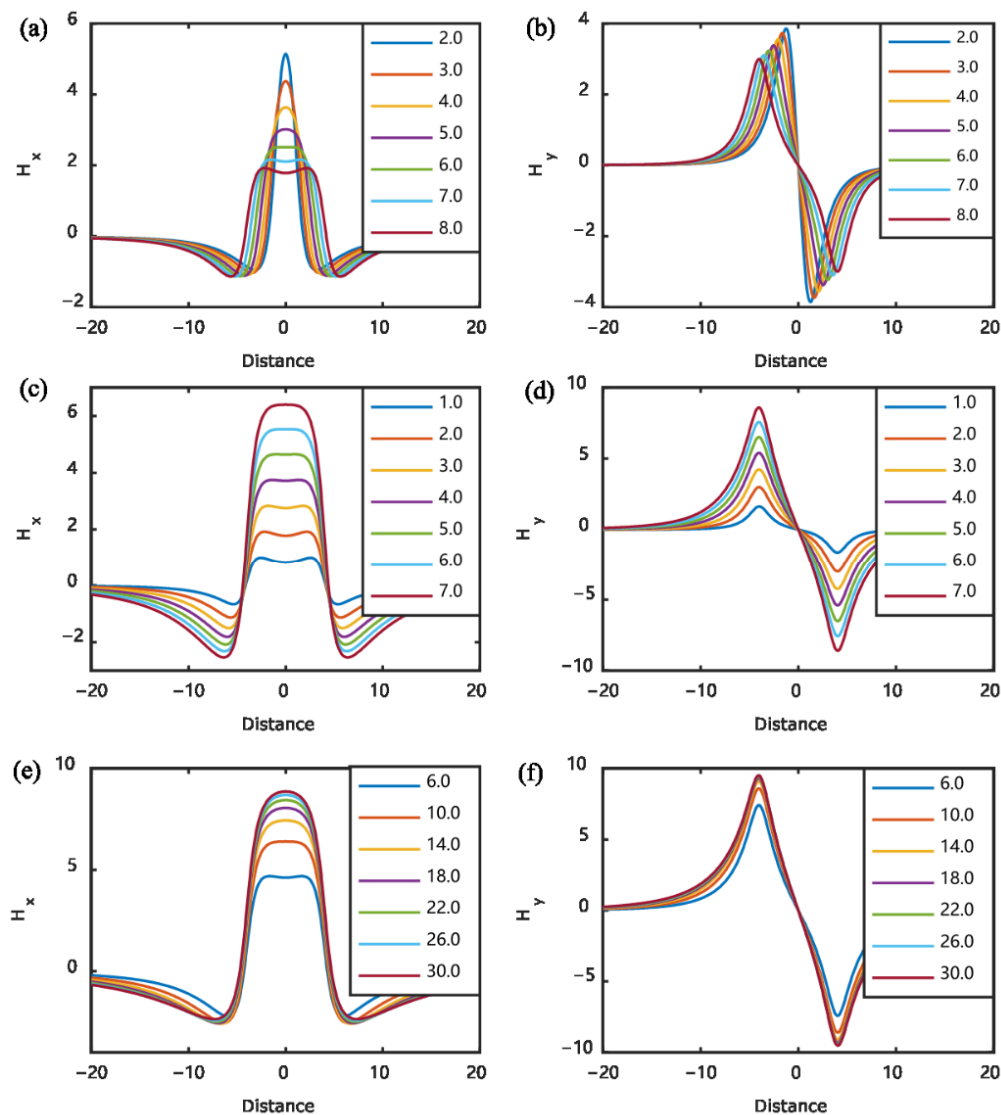


Figure 5. Influences of defect dimensions on MFL signal: (a) change in H_x with defect width; (b) change in H_y with defect width; (c) change in H_x with defect depth; (d) change in H_y with defect depth; (e) change in H_x with defect length; (f) change in H_y with defect length.

Conventionally, researchers and engineers of MFL have thought that the orientation defect should be perpendicular to the magnetization field to obtain an effective MFL field. Sun and Song questioned this traditional conclusion and studied the MFL signals for defects parallel to the magnetization field [30,31]. They found that it was possible to detect cracks that are parallel to the magnetization, although the amplitude was small. Wu further studied the variation of MFL signal amplitude with the angle between the defect and magnetization field [32], the results are shown in Figure 6.

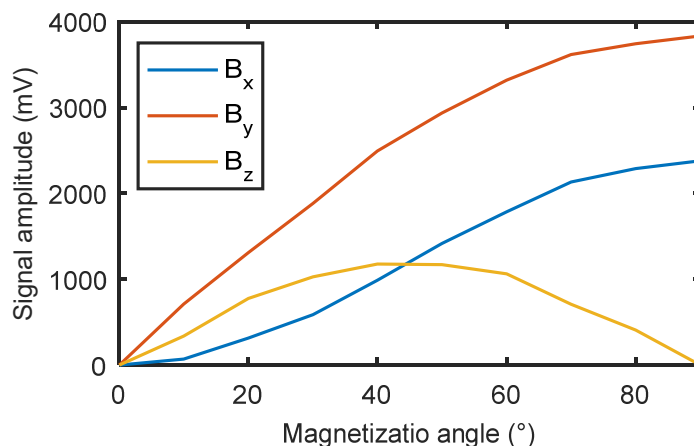


Figure 6. Influence of the angle between magnetization and defect on MFL signal.

The scanning direction of the sensors also influences the MFL signal, and Wu also studied this effect [32]. This effect can also be obtained by extracting the magnetic field along different directions using Equations (4)–(6). For a defect with the dimensions $a = 1$, $b = 2$, and $c = 10$, the variation of the MFL signal with scanning direction is shown in Figure 7.

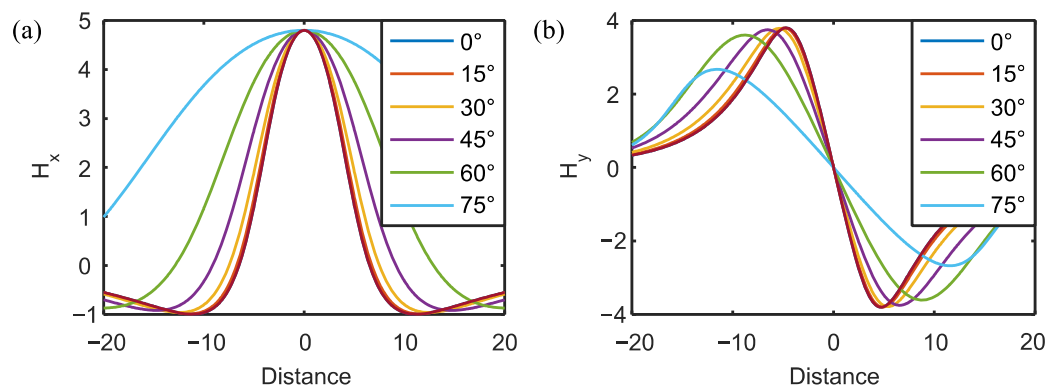


Figure 7. Influence of scanning angle on MFL signal: (a) change in H_x with scanning angle; (b) change in H_y with scanning angle.

3.2. Liftoff Effect

The MFL signal is dependent on the liftoff distance between the probe and the specimen. The MFL signal reduces as the increase in liftoff distance [33–35], an example of liftoff effect is shown in Figure 8.

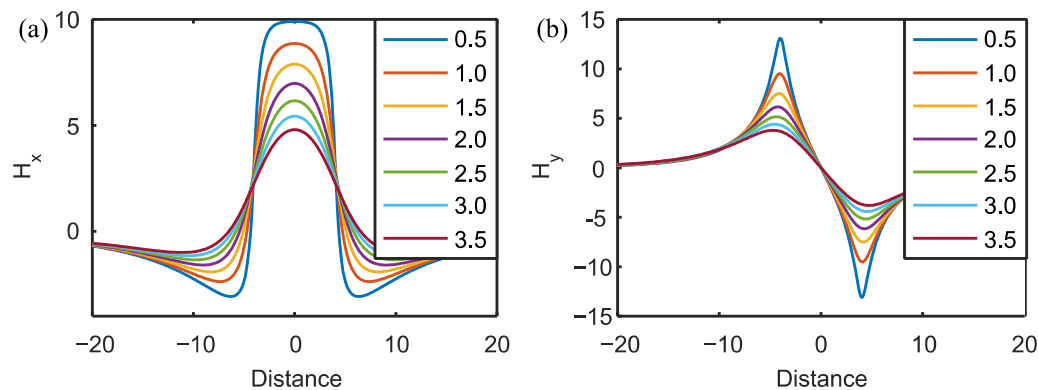


Figure 8. Influence of liftoff on MFL signal: (a) change in H_x with liftoff; (b) change in H_y with liftoff.

The change in liftoff during scanning significantly influences the testing signal. Thus, many researchers have attempted to reduce the liftoff effect. Jia used a filtering method to suppress liftoff interference [36]; Wu proposed a liftoff tolerant sensor by inserting ferrite into the sensing coil [37]; Peng introduced an exponential function compensation for liftoff correction [38]; Wang linearized the liftoff effect by applying Fourier transform [39].

3.3. Magnetization Strength and Material Property

Usually, a strong magnetization is required to saturate the ferromagnetic material to obtain a good MFL signal. However, the MFL signal does not always increase with magnetization strength. Many researchers have found that the MFL signal initially increases with the magnetizing current and starts to decrease after a certain point [40–42], as shown in Figure 9. Sun explained this phenomenon with the magnetic compression effect [43], which states that the large background field caused by strong magnetization suppresses the leakage of the magnetic field from defects. Later, he proposed a new MFL principle based on near-zero background magnetic field [44], in which magnetic shielding is used to collect a strong background field.

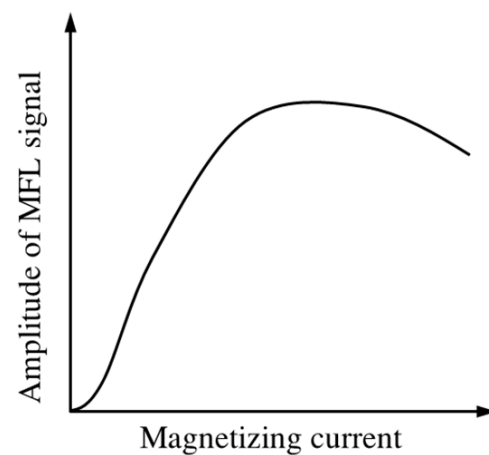


Figure 9. Influence of magnetizing current on MFL signal.

Since the magnetization of the material is also based on the material property, the MFL signal is also dependent on the B–H curve of the ferromagnetic materials. Katoh approximated the B–H curve with two lines and studied this influence [45].

3.4. Velocity Effect

In pipeline inspection, the MFL device is propelled by the gas and oil inside the pipe. The device usually travels several meters per second. Due to the relatively motion between the magnetizer and the pipe, eddy currents are induced in the pipe wall. The motion-induced eddy current density is:

$$\mathbf{J} = \sigma \mathbf{v} \times \mathbf{B} \quad (8)$$

The eddy currents generate a secondary magnetic field according to the Biot–Savart law. Thus, the magnetization status of the pipe and corresponding MFL signal will be affected at high testing speeds. The problem is governed by Maxwell’s equations considering the velocity term:

$$\nabla^2 \mathbf{B} - \mu \sigma \frac{\partial \mathbf{B}}{\partial t} - \mu \sigma (\mathbf{v} \cdot \nabla) \mathbf{B} = 0 \quad (9)$$

Many researchers have studied the velocity effect of finite element simulation. For the yoke-type magnetizer, the eddy currents are induced in the region beneath the poles [46–49], and the magnetic field is perturbed [50]. A comparison between the distributions of the eddy current and magnetic field at different speeds is shown in Figure 10.

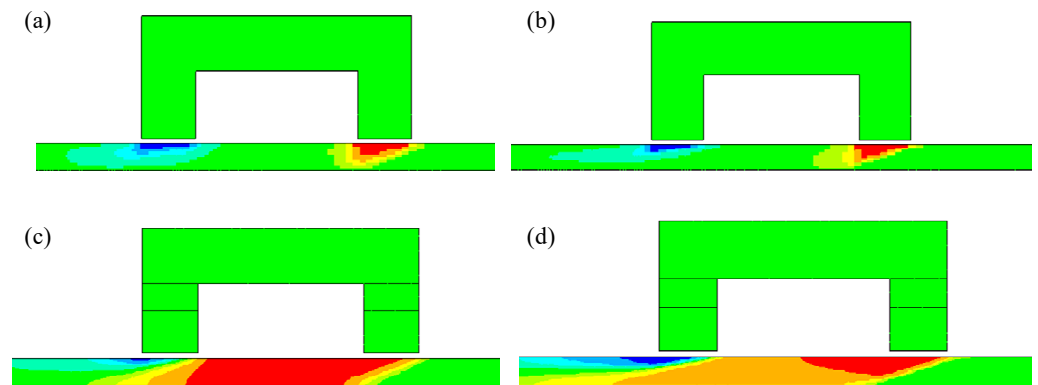


Figure 10. Distribution of motion-induced eddy current and magnetic field: (a) eddy current at 0.5 m/s; (b) eddy current at 2 m/s; (c) magnetic field at 0.5 m/s; (d) magnetic field at 2 m/s.

Recently, B. Feng found an analytical solution to Equation (9) and further obtained the expression of the motion-induced eddy current under a pole of the magnetizer [51]:

$$J_{\text{total}} = \frac{1}{\pi} \cdot \int_0^{\infty} dk \int_{y_0}^{y_0+h} \left[\frac{1}{\mu} (jkC_y^{\text{III}} e^{ky} + jkD_y^{\text{III}} e^{-ky} - kIC_x^{\text{III}} e^{ky} + kID_x^{\text{III}} e^{-ky}) \right] e^{jkx} dy' \quad (10)$$

where J_{total} is the eddy current in specimen, y_0 is the liftoff, h is the height of magnetizer, C_x^{III} , C_y^{III} , D_x^{III} and D_y^{III} are coefficients that are solved as [51]:

$$C_x^{\text{III}} = -\frac{2j\mu IkI(kI+k)e^{-kyI+ktI} \sin(ka)}{e^{ktI}(kI+k)^2 - e^{-ktI}(kI-k)^2}$$

$$D_x^{\text{III}} = \frac{2j\mu IkI(kI-k)e^{-kyI-ktI} \sin(ka)}{e^{ktI}(kI+k)^2 - e^{-ktI}(kI-k)^2}$$

$$C_y^{\text{III}} = -\frac{2\mu Ik(kI+k)e^{-kyI+ktI} \sin(ka)}{e^{ktI}(kI+k)^2 - e^{-ktI}(kI-k)^2}$$

$$D_y^{\text{III}} = -\frac{2\mu Ik(kI-k)e^{-kyI-ktI} \sin(ka)}{e^{ktI}(kI+k)^2 - e^{-ktI}(kI-k)^2}$$

With the analytical solution of the MIEC, the tail effect and tilt angle of the MIEC at different moving speeds are also analyzed [51].

The encircling coil-type magnetizer is more commonly used in the manufacturing line for the inspection of steel pipes. As the production speed increases, there is also a need for high-speed testing. For the encircling coil-type magnetizer, the motion-induced eddy currents are mainly focused on the edge of the magnetizing coil [52–56]. Wu also studied the distribution of eddy current in circumferential-type MFL testing [57].

The influence of the velocity on the MFL signal has also been extensively studied. There are changes in both the signal baseline and signal amplitude, and the signal shape is also distorted [58–61]. The change in MFL signal amplitude with velocity has been reported in many previous studies, some have reported that the signal amplitude decreases with the increase in velocity [48,52]. However, further detailed analyzes by Pullen showed that when there is insufficient flux saturating the specimen, the MFL signal for far-side defects decreases with scanning speed, while the signal for near-side defects increases with the speed [62,63]. Zhang further found that the influence of the velocity also depends on the sensor position [64]. In order to reduce the velocity impact, Usarek studied the change in the magnetic field with velocity and found that both tangential and normal components of the magnetic field increase with velocity linearly and used an empirical fitting equation to compensate for the MFL signal [65].

Based on the studies of the velocity effect in MFL testing, many researchers have attempted to use the velocity-induced field for testing. Antipov used an induced tail magnetic field to test rails at high-speed [66]. B. Feng, T. Rocha, and F. Yuan all studied the motion-induced eddy current testing method and used magnetic field sensors to pick up the defect signals [51,67–72]. Researchers from Technische Universität Ilmenau proposed a new Lorentz force NDT method for conductive specimens, which is also based on motion-induced eddy current [73–77].

3.5. Other Effects

In MFL testing, there are also other factors that influence the MFL signal, such as stress, surface roughness, corrosion coverage, and probe gesture. Kasai studied the MFL testing signal for samples covered by corrosion (iron oxides) and showed that the MFL signal decreased with increasing iron oxide ratio [78]. Long studied the influence of gesture probes on MFL signal and proposed a dual magnetic sensor model to compensate for the change in probe gesture [79].

The stress effect has been studied by many researchers [80–91]. The properties of ferromagnetic materials change with the loading stress due to the magneto-mechanical coupling, thus the MFL signal also changes with the stress. Y. Wang proposed a multi-physics simulation model to study the change in MFL signal with stress and showed that the peak-to-peak amplitude of the normalized MFL signal decreases with an increase in stress [80]. Mandal showed that the circumferential bending stress changes the magnetic easy axis of the pipe and thus reduces the MFL signal [81]. Y. Wang also studied the stress-dependent MFL signals in Q235 steel plates [82]. Timoshenko's theory and the J-A model were combined to calculate the stress-dependent distribution of magnetization, then a modified magnetic dipole model considering the stress dependence was proposed. With the proposed model, Wang showed that the MFL signal increases with the increase in stress in the Q235 steel plate. Gao also observed a similar effect in the testing of steel wire ropes [83]. Later, Shi showed that the change in the MFL signal behaves differently in the elastic and plastic deformation stage [84].

For the testing of micro-cracks, the influences of surface roughness cannot be ignored. Deng considered the rough surface as concave and convex defects and showed that a rough surface introduces background noise to the MFL signal and reduces the signal-to-noise ratio (SNR) [92]. Yang also studied the effect of surface roughness on the SNR of MFL signals and proposed the use of a magnetic medium to improve the SNR [93]. In another study, B.P.C. Rao proposed the use of an Eigen vector-based approach to suppress the noise caused by non-linear permeability, surface roughness, stresses, and liftoff variations in MFL images [94]. Since the surface roughness influences the MFL signal, the MFL signal can be used in turn to represent the surface roughness. Li proposed to use the MFL signal and its spatial Fourier spectrum to measure surface roughness [95].

4. Excitation and Sensing Techniques in MFL Testing

4.1. Excitation Methods

4.1.1. Structures of Magnetizer

In conventional MFL testing, the excitation field is provided by either permanent magnets or direct current (DC) carrying coils. The main advantages of using permanent magnets include: (1) the magnetizer has a relatively small size and light weight; (2) there is no need for an external power supply. Due to these features, magnet-based magnetizers are especially suitable for use in portable devices and inspection robots for the inspection of wire ropes and transmission pipelines. The drawback of using permanent magnets is that the installation is not convenient due to the large magnetic force between the magnet and the specimen, and the magnetization strength is difficult to adjust. These drawbacks can be overcome using coils. The magnetization strength can be easily adjusted by changing the current in the coil and the current can be turned off during the installation. The distribution of the magnetic field generated by magnetizing coils can be calculated through

magnetic vector potentials [96], and a uniform magnetizing field can be achieved by the design of Helmholtz coils [97]. However, coil-based magnetizers usually have larger sizes; thus, they have limitations in some applications. With either a permanent magnet or coil, a ferromagnetic yoke can be used to formulate magnetic circuits with less magnetic reluctance to increase the magnetization inside the specimens.

The encircling coil-based magnetizer has the advantage of providing a strong and adjustable magnetizing field; however, wires are closed, making it difficult for certain specimens such as wire ropes and coiled tubing to be inserted into the middle of the coil. To solve this problem, Y. Sun proposed an opening electromagnetic transducer, as shown in Figure 11, which facilitates the insertion of specimens [98,99]. S. Wang proposed a flexible magnetizer-based parallel cable that may have potential applications in specimens with complex curvature [100].

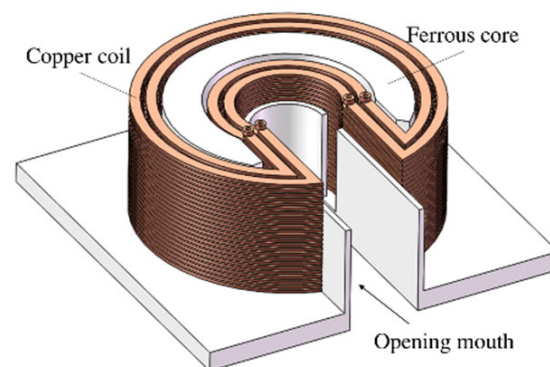


Figure 11. The structure of the opening electromagnetic transducer.

For the yoke type magnetizer, Y. Chang did several optimizations for the yoke shape, yoke size and thickness of shielding layer with the help of finite element simulation [101]. J. Parra-Raad performed a multi-object optimization for pipeline inspection gauge (PIG) by the genetic algorithm [102]. The conventional yoke type magnetizer only generates a magnetic field in one direction and has limited sensitivity for cracks that are parallel to the magnetic field. A double U-shaped orthogonal magnetizer, as shown in Figure 12, can be used to overcome this problem, although it was originally developed for alternating current field measurement (ACFM) [103]. When AC excitation is used in the MFL testing, the direction of the magnetizing field can be adjusted by controlling the phase difference between the two yokes.

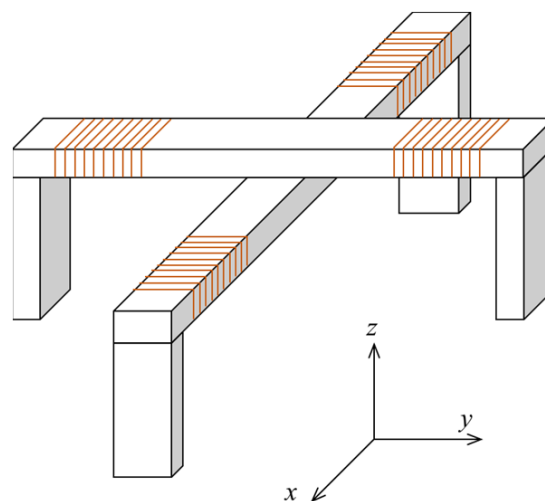


Figure 12. The structure of double U-shaped orthogonal magnetizer.

4.1.2. Excitation Signal Waveforms

To extract more defect information in MFL testing, researchers have considered the optimization of the excitation signal waveform. Alternating current magnetic flux leakage (ACMFL), pulsed magnetic flux leakage (PMFL), and MFL-based combined AC and DC excitation have been proposed. Y. Gotoh conducted a comprehensive study on ACMFL, analyzed ACMFL with finite element simulation, stated the necessity of using nonlinear analysis, and used the method to detect plural cracks [104,105]. Due to the skin effect, the magnetic field concentrates on the surface of the specimen, thus the surface can be saturated with a relatively small excitation current. Gotoh also used low-frequency AC excitation to increase the penetration depth and detected outer side cracks in a steel plate 3 mm thick [106,107]. Hayashi proposed an unsaturated ACMFL testing method for reinforcing steel bars and achieved defect inspection at high liftoff of up to 100 mm [108].

To increase the depth of penetration and obtain richer information, A. Sophian and G.Y. Tian proposed the PMFL method, in which a square waveform is applied as the excitation signal [109]. It was found that the PMFL method has advantages in defect location and sizing. J. Wilson combined the PMFL method with pulsed magnetic reluctance (PMR), which provided a complementary approach for the integrated inspection of surface and sub-surface cracks [110]. Subsequently, many researchers have studied the signal characteristics and extracted features for defect quantification and discrimination of internal and external defects [111–114].

The combined DC and AC excitation has also been used in MFL testing. D. Wu proposed a magnetizer with both permanent magnets and coils excited with alternating current [115]. The AC excitation was used to generate eddy currents that were perpendicular to the DC magnetic field to cover the blind zone of the DCMFL. R. Wang proposed to use two encircling coils to, respectively, generate DC and AC magnetizing fields [116], in which the DC field is used to set the working point by changing the permeability and the AC field is used to obtain the defect information. The results showed that this method can be used to increase the detectability of internal defects. Y. Gotoh also studied the combinational use of DC and AC excitation and took into account the minor hysteresis loop in the detection of far-side defects [117].

4.2. Sensing Methods

After generating a leakage field with appropriate excitation, sensing is the vital step to pick up the leakage field. Various types of magnetic field sensors that can convert the magnitude of a magnetic field into the corresponding voltage have been used in MFL testing. The most commonly used sensors are the Hall element and coils. Hall element is able to measure the absolute value of the magnetic field; however, when the sensor is near the poles of the magnetizer, it may operate outside the linear range. Coils have a wider measurement range; however, they only measure the rate of change in the magnetic field instead of its absolute value. In recent studies, magnetic field sensors with higher sensitivities have been used in MFL testing for the detection of tiny cracks. Kataoka and Singh used a giant magnetoresistance (GMR) line sensor and flexible GMR sensor array in MFL [118,119]. Tehranchi used a double-core giant magneto-impedance (GMI) sensor in the testing of steel plates [120]. Z. Jin used a tunnel magnetoresistance (TMR) sensor for the inspection of steel bars [121]. Kallias and Krause discussed the potential of using a superconducting quantum interference device (SQUID) in nondestructive testing [122,123].

In addition to using new sensing elements, researchers have also tried to enhance the MFL signal by the design of a probe structure. G. Park and Y. Jia both considered adding a ferromagnetic backing near the sensor to enhance the MFL signal [124,125]. J. Wu proposed to use a magnetic head (as shown in Figure 13) to detect tiny cracks in bearings [126], J. Tang further studied the influence of head pose on the MFL signal [127]. E. Li studied the relationship between the size of the opening in the magnetic head and the frequency of the MFL signal and designed a magnetic head structure for trans-scale defects [128,129]. S. Liu proposed a magnetic focusing sensor that adds a magnetic guide core and a permanent

magnet to coils [130]. D. Wu proposed to use two sensors to measure the change rate of magnetic flux leakage to reduce background and vibration noises [131]. J. Tang proposed to use a ferromagnetic material with grooves to replace the conventional non-ferromagnetic liftoff layer to increase the MFL signal [132]. T. Nara designed a Fourier coil consisting of two coils of radial offset [133]. The sensor is able to obtain the Fourier coefficients of the leakage magnetic flux and locate the center of the crack.

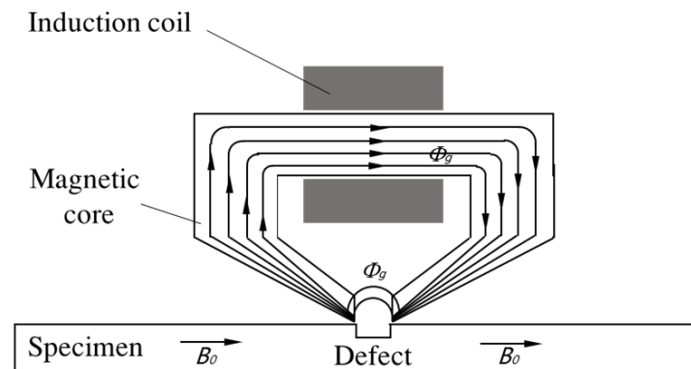


Figure 13. The structure of magnetic head.

Magnetic sensors are the most commonly used sensing methods in MFL testing; however, the results are not intuitive, and it requires additional signal processing circuits and display modules. J. Philip and V. Mahendran have proposed the use of a ferrofluid emulsion film to visualize the leakage magnetic field [134–136]. The uniformly distributed particles re-distribute under the leakage magnetic field and exhibit different colors due to Bragg scattering of the droplets. J. Lee also proposed a method to visualize the leakage magnetic field using magneto-optical film (MOF) [137]. According to the magneto-optical effect, a polarized light rotates when it is transmitted through an MOF with an external field, and the rotated angle is proportional to the external field. Thus, the MOF can be used to observe the leakage magnetic field. M. Tehranchi added a detector behind the magneto-optical sensor to capture the light and recorded the change in the magnetic field in a computer [138].

The development of the sensing method in MFL is mainly dedicated to the inspection of micro-cracks, especially the cracks in high-precision mechanical parts such as bearing and bearing roller. Researchers have optimized the sensing probe from the aspects of using highly sensitive sensors such as TMR and designing new types of structures such as magnetic heads [126,128]. In E. Li's paper, it is reported that the smallest crack that can be detected is with a depth of 7 μm .

5. Inverse Problem in MFL and Defect Quantification

The ultimate goal of non-destructive testing can be classified into three levels. At the basic level, we need to determine whether there are defects in the specimen based on the testing signals. Furthermore, the defect size needs to be quantified to determine the severity of the damage. Ultimately, the defect size information will be used to predict the remaining life of the structures. After decades of development, qualitative determination of the existence of a defect is relatively simple. Thus, a lot of effort has been put into the study of the quantification of defects, which is a classical inverse problem.

5.1. Machine Learning-Based Defect Quantification

Machine learning has undergone rapid development in recent years, especially in the branches of artificial neural networks (ANN) and deep learning. Machine learning techniques showed great success in tasks such as classification and regression. The task of defect quantification is essentially a problem of classification or regression; thus, artificial neural networks have been widely used in defect quantification in MFL testing. The

neural networks can be regarded as a function that maps the inputs (raw signal or features extracted from the signal) to the outputs (defect type, defect size, etc.). To train a neural network, experiments and simulations should be conducted for defects of various sizes. The defect sizes and corresponding signals (or signal features) are fed into the network to update the weights.

Initially, due to the limited performance of computers, shallow neural networks with one or two hidden layers were used. Carvalho used raw MFL signals and signals after filtering as the input to the neural network, and classified signals into defects and non-defects with an accuracy of 94.2% [139]. He also used the neural network to classify the defects into external corrosion, internal corrosion, and lack of penetration with an accuracy of 71.7%. K. Hwang employed the wavelet basis function (WBF) neural network to the MFL signal to a three-dimensional defect profile [140]. The WBF provides a multi-resolution approximation and overcomes some disadvantages of the radial basis function neural network. Khodayari-Rostamabad introduced various machine learning techniques and feature selection methods and estimated the defect depth with an error of less than 8% [141]. Kandroodi used the MFL signal contour to determine the defect length and width and used the signal peak-to-peak values along with the estimated length and width to estimate the defect depth [142].

With the increase in computer performance, deep neural networks that require massive computational resources have been applied in many industrial fields. The additional layers in the deep neural network can be regarded as feature extractors. Applying deep neural networks avoids manual feature extraction, a process that highly depends on the experience of the researcher and the engineer. J. Feng applied a convolutional neural network (CNN) to classify injurious and noninjurious defects based on MFL images and showed that CNN gave more accurate predictions than neural networks, support vector machines, decision trees, and correlation-based methods [143]. S. Lu proposed a visual transformation CNN for defect quantification and improved the accuracy of estimation for length, width, and depth by 26.9%, 27.1%, and 33.3% [144]. Z. Wu used reinforcement learning to replace the classic iteration process and successfully reconstructed complex defect depth profiles [145]. H. Sun stated that taking into account the physical concepts in the deep neural network would be better than only using general neural networks [146]. He integrated the MFL theory into the loss function and proposed a physics-informed doubly fed cross-residual network that estimated the defect length, width, and depth accurately [146].

5.2. Iteration-Based Defect Quantification

Prior to the application of machine learning-based methods, iteration-based methods have been widely used in defect quantification [147–159]. The basic concept of iteration methods is shown in Figure 14, where the defect quantification is regarded as an optimization problem that minimizes the difference between the experimentally measured MFL signal and the one calculated with the estimated defect profile. To begin the defect quantification process, an initial estimate of the defect profile is required. Then, a forward MFL model is used to calculate the MFL signal generated by the defect profile. Usually, there are types of forward models that can be used, namely the magnetic dipole model, finite element model, and neural network model. After the calculation with the forward model, a comparison is made between the calculated MFL signal and the one obtained in the experiment. If the error is less than a desirable value, the profile will be regarded as the final estimation, otherwise, the error is used to update the defect profile and repeat the process of forward calculation.

Since defect quantification is regarded as an optimization problem, many optimization algorithms can be used to update the defect profiles. More conventionally, the gradient descent algorithm is used [160–162]. Later, genetic algorithms [162], particle swarm optimization [163–165], and cuckoo search [166,167] have been applied to quantify defects in MFL testing.

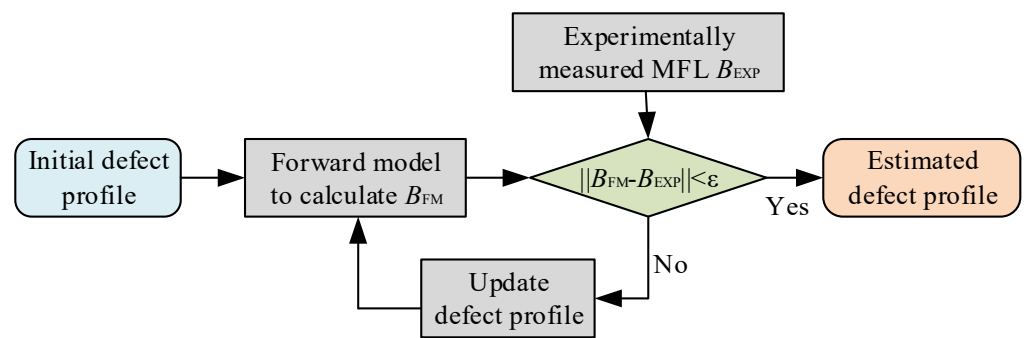


Figure 14. The iterative process for defect quantification in MFL testing.

6. Applications and Comparison with Related NDT Methods

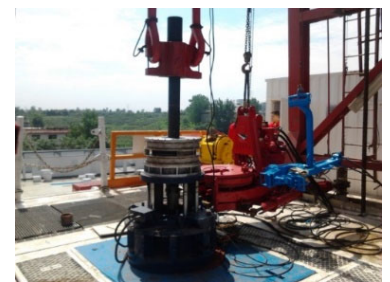
6.1. Applications of MFL Testing

As an efficient nondestructive testing method for ferromagnetic materials, MFL testing has been successfully applied in many industrial fields. One of the most important applications is underground pipeline inspection, where the so-called pipeline inspection gauge (PIG) is used. The PIG usually has permanent magnets as the magnetizing units, ferromagnetic yokes to connect the magnets and form a magnetic circuit, and brushes to separate the magnetizer and pipes.

Another important application is the inspection of steel pipes during manufacturing. According to the API standard, the steel pipes must be tested before leaving the factory. Among the testing methods, the MFL is the most commonly used. Typical MFL equipment for seamless steel pipe is shown in Figure 15a. It consists of three modules, two of which are for the inspection of transverse and longitudinal cracks and a demagnetizing module to demagnetize the pipe after inspection. For the inspection of transverse cracks, encircling coils have been used to generate axial magnetic fields in steel pipes. For the inspection of longitudinal cracks, magnetizers with two shoes that are 180° away from each other are used to generate magnetic fields in the circumferential direction. In the oil industry, MFL has also been applied in the inspection of drill pipes and sucker rods as shown in Figure 15b,c.



(a)



(b)



(c)



(d)

Figure 15. Applications of MFL: (a) seamless steel pipe; (b) drill pipe; (c) sucker rod; (d) bearing.

In the automobile industry, bearings were previously tested by the method of magnetic particle inspection (MPI). MPI has good sensitivity for tiny cracks; however, the inspection result is dependent on the analysis of the inspector. With the usage of highly sensitive sensors, MFL can also achieve the detection of tiny cracks. In addition, MFL has the advantage of automatic inspection; thus, it is replacing MPI in several fields, such as the inspection of bearing, as shown in Figure 15d.

In industrial applications, usually, an array of magnetic sensors is used to cover the whole area of the specimen. There are two common ways to display and visualize multi-channel signals. The most typical way is to display the signals one by one in the time domain as shown in Figure 16a. With the rapid development of image processing technology, especially deep learning techniques such as CNN, displaying the MFL testing results as gray-scale images (Figure 16b) would facilitate the application of corresponding algorithms to extract defect information.

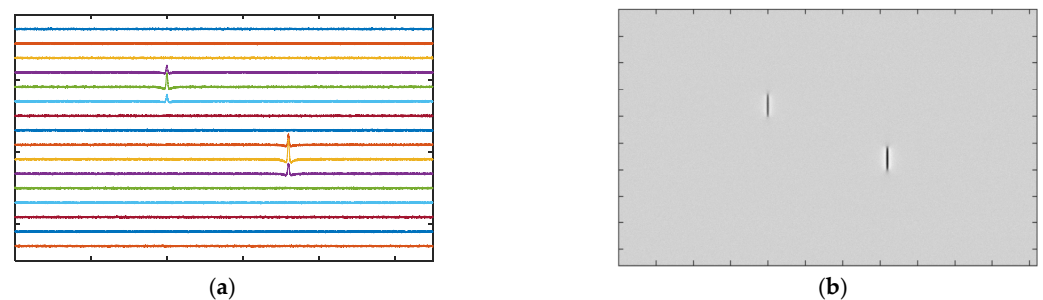


Figure 16. Visualizing MFL testing signals: (a) multi-channel time-domain signals; (b) gray-scale images.

6.2. Comparison with Related NDT Methods

MFL technique belongs to the category of electromagnetic NDT. Within this category, there are other methods such as eddy current testing (ECT), magnetic particle inspection (MPI), metal memory method (MMM), magnetic Barkhausen noise (MBN) method, permanent perturbation (PMP) method, magnetic adaptive testing (MAT) method, and magnetic permeability perturbation (MPP) method. The advantage of MFL over MPI is the easiness of implementing automatic testing; however, at the same time, it has lower sensitivity than MPI. When compared with ECT, MFL has better detection ability for deeply buried defects, whereas it has lower sensitivity for surface defects.

The comparison between MFL and newly proposed electromagnetic NDT methods has been discussed in some previous publications. G. Vértesy applied MFL, MMM, and MAT to detect an artificial slot in stacked steel plates, he found that the MFL gave good results when there are one or two layers and MAT outperformed MFL when there were more layers [168]. Z. Deng compared MFL with MPP and found that MPP can detect defects that are buried deeper than MFL [169]. Y. Sun compared MFL with PMP and stated that the PMP method can accomplish inspection in a narrower operation space and is more suitable for omni-directional cracks [170,171].

7. Conclusions

In this paper, a comprehensive review of the MFL technology has been presented. Firstly, the principle of MFL testing has been explained with the theory of refracted magnetic field and an analytical expression for the leakage magnetic field has been derived based on the 3D magnetic dipole model. Then, the influence of some crucial factors, such as defect size, defect orientation, liftoff distance, magnetization strength, testing speed, surface roughness, and stress, on the MFL testing signal has been analyzed.

Excitation and sensing are the most important steps in MFL testing, in which excitation decides if there is a leakage field generated, and sensing decides if the generated field can

be effectively detected. In this paper, the development of magnetizer structures and the usage of different excitation signal waveforms have been introduced.

In the quantification of defects, there are mainly two types of algorithms, namely the machine learning-based algorithm and the iteration-based algorithm. Both algorithms achieved relatively good accuracy on defect quantification. The machine learning-based algorithm usually requires a large training set, and the iteration-based algorithm usually requires large computational resources during the iteration process.

With the advantages of high efficiency, low cost, and environmental friendliness, MFL has been applied in many applications such as underground pipelines, seamless steel piles, drill pipes, sucker rods, and bearings.

Author Contributions: Conceptualization, B.F. and J.W.; writing—original draft preparation, B.F., H.T. and J.T.; writing—review and editing, J.W. and Y.K.; funding acquisition, B.F. and J.W. All authors have read and agreed to the published version of the manuscript.

Funding: This research was funded by the National Natural Science Foundation of China, grant numbers 52105551 and 92060114, Fundamental Research Funds for the Central Universities, grant number HUST: 2020kfyXJJS015, and Sichuan Science and Technology Program grant number 2022YFS0524 and 2022YFG0044.

Institutional Review Board Statement: Not applicable.

Informed Consent Statement: Not applicable.

Data Availability Statement: Not applicable.

Conflicts of Interest: The authors declare no conflict of interest.

References

1. Shi, Y.; Zhang, C.; Li, R.; Cai, M.; Jia, G. Theory and Application of Magnetic Flux Leakage Pipeline Detection. *Sensors* **2015**, *15*, 31036–31055. [[CrossRef](#)] [[PubMed](#)]
2. Wang, Z.D.; Gu, Y.; Wang, Y.S. A Review of Three Magnetic NDT Technologies. *J. Magn. Magn. Mater.* **2012**, *324*, 382–388. [[CrossRef](#)]
3. Liu, S.; Sun, Y.; Gu, M.; Liu, C.; He, L.; Kang, Y. Review and Analysis of Three Representative Electromagnetic NDT Methods. *Insight* **2017**, *59*, 176–183. [[CrossRef](#)]
4. Ma, Q.; Tian, G.; Zeng, Y.; Li, R.; Song, H.; Wang, Z.; Gao, B.; Zeng, K. Pipeline In-Line Inspection Method, Instrumentation and Data Management. *Sensors* **2021**, *21*, 3862. [[CrossRef](#)]
5. Sun, Y.; Kang, Y. Magnetic Mechanisms of Magnetic Flux Leakage Nondestructive Testing. *Appl. Phys. Lett.* **2013**, *103*, 184104. [[CrossRef](#)]
6. Zatspein, N.; Shcherbinin, V. Calculation of the magnetostatic field of surface defects, I. Field topography of defect models. *Defektoskopiya* **1966**, *5*, 50–59.
7. Shcherbinin, V.; Pashagin, A. Influence of the extension of a defect on the magnitude of its magnetic field. *Defektoskopiya* **1972**, *8*, 74–82.
8. Förster, F. New Findings in the Field of Non-Destructive Magnetic Leakage Field Inspection. *NDT Int.* **1986**, *19*, 3–14. [[CrossRef](#)]
9. Edwards, C.; Palmer, S.B. The Magnetic Leakage Field of Surface-Breaking Cracks. *J. Phys. D Appl. Phys.* **1986**, *19*, 657–673. [[CrossRef](#)]
10. Uetake, I.; Saito, T. Magnetic Flux Leakage by Adjacent Parallel Surface Slots. *NDT E Int.* **1997**, *30*, 371–376. [[CrossRef](#)]
11. Dutta, S.M.; Ghorbel, F.H.; Stanley, R.K. Simulation and Analysis of 3-D Magnetic Flux Leakage. *IEEE Trans. Magn.* **2009**, *45*, 1966–1972. [[CrossRef](#)]
12. Dutta, S.M.; Ghorbel, F.H.; Stanley, R.K. Dipole Modeling of Magnetic Flux Leakage. *IEEE Trans. Magn.* **2009**, *45*, 1959–1965. [[CrossRef](#)]
13. Mandache, C.; Clapham, L. A Model for Magnetic Flux Leakage Signal Predictions. *J. Phys. D Appl. Phys.* **2003**, *36*, 2427–2431. [[CrossRef](#)]
14. Lukyanets, S.; Snarskii, A.; Shamonin, M.; Bakaev, V. Calculation of Magnetic Leakage Field from a Surface Defect in a Linear Ferromagnetic Material: An Analytical Approach. *NDT E Int.* **2003**, *36*, 51–55. [[CrossRef](#)]
15. Trevino, D.A.G.; Dutta, S.M.; Ghorbel, F.H.; Karkoub, M. An Improved Dipole Model of 3-D Magnetic Flux Leakage. *IEEE Trans. Magn.* **2016**, *52*, 1–7. [[CrossRef](#)]
16. Huang, X.; Wu, J.; Sun, Y.; Kang, Y. 3D Magnetic Dipole Models of Magnetic Flux Leakage for “concave” and “Bump” Defects. *Int. J. Appl. Electromagn. Mech.* **2019**, *59*, 1305–1312. [[CrossRef](#)]

17. Zhang, Y.; Sekine, K.; Watanabe, S. Magnetic Leakage Field Due to Sub-Surface Defects in Ferromagnetic Specimens. *NDT E Int.* **1995**, *28*, 67–71. [[CrossRef](#)]
18. Li, H.; Chen, Z.; Zhang, D.; Sun, H. Reconstruction of Magnetic Charge on Breaking Flaw Based on Two-Layers Algorithm. *Int. J. Appl. Electromagn. Mech.* **2016**, *52*, 1133–1139. [[CrossRef](#)]
19. Bowler, J.R.; Bowler, N. Evaluation of the Magnetic Field near a Crack with Application to Magnetic Particle Inspection. *J. Phys. D Appl. Phys.* **2002**, *35*, 2237–2242. [[CrossRef](#)]
20. Cheng, Y.; Wang, Y.; Yu, H.; Zhang, Y.; Zhang, J.; Yang, Q.; Sheng, H.; Bai, L. Solenoid Model for Visualizing Magnetic Flux Leakage Testing of Complex Defects. *NDT E Int.* **2018**, *100*, 166–174. [[CrossRef](#)]
21. Wang, Y.; Cheng, Y.; Bai, L.; Zhang, J.; Yu, H.; Alimey, F.J. Solenoid Model for the Magnetic Flux Leakage Testing Based on the Molecular Current. *IEEE Trans. Magn.* **2018**, *54*, 1–14. [[CrossRef](#)]
22. Huang, S.L.; Peng, L.; Wang, S.; Zhao, W. A Basic Signal Analysis Approach for Magnetic Flux Leakage Response. *IEEE Trans. Magn.* **2018**, *54*, 6201906. [[CrossRef](#)]
23. Suresh, V.; Abudhair, A. Dipole Model to Predict the Rectangular Defect on Ferromagnetic Pipe. *J. Magn.* **2016**, *21*, 437–441. [[CrossRef](#)]
24. Wang, Y.; Xu, Y.; Ding, S.; Dai, G.; Liu, Y.; Yang, Z.; Liu, F. Numerical Simulation and Experiment on Magnetic Flux Leakage Inspection of Cracks in Steels. In Proceedings of the 17th World Conference on Nondestructive Testing, Shanghai, China, 25–28 October 2008; pp. 1–5.
25. Ji, F.; Wang, C.; Sun, S.; Wang, W. Application of 3-D FEM in the Simulation Analysis for MFL Signals. *Insight Non-Destr. Test. Cond. Monit.* **2009**, *51*, 32–35. [[CrossRef](#)]
26. Pearson, N.R.; Boat, M.A.; Priewald, R.H.; Pate, M.J.; Mason, J.S.D. A Study of MFL Signals from A Spectrum of Defect Geometries. In Proceedings of the 18th World Conference on Nondestructive Testing, Durban, South Africa, 16–20 April 2012; pp. 16–20.
27. Atherton, D.L.; Daly, M.G. Finite Element Calculation of Magnetic Flux Leakage Detector Signals. *NDT Int.* **1987**, *20*, 235–238. [[CrossRef](#)]
28. Katragadda, G.; Si, J.T.; Lord, W.; Sun, Y.S.; Udpa, S.; Udpa, L. A Comparative Study of 3D and Axisymmetric Magnetizer Assemblies Used in Magnetic Flux Leakage Inspection of Pipelines. *IEEE Trans. Magn.* **1996**, *32*, 1573–1576. [[CrossRef](#)]
29. Huang, S.; Li, L.; Yang, H.; Shi, K. Influence of Slot Defect Length on Magnetic Flux Leakage. *J. Mater. Sci. Technol.* **2004**, *20*, 231–232.
30. Sun, Y.; Kang, Y. The Feasibility of MFL Inspection for Omni-Directional Defects under a Unidirectional Magnetization. *Int. J. Appl. Electromagn. Mech.* **2010**, *33*, 919–925. [[CrossRef](#)]
31. Song, K.; Kang, Y.; Sun, Y.; Qiu, C.; Su, J. MFL Testing of Omni-Directional Cracks in Steel Strip Using Strong Longitudinal Magnetization. *Int. J. Appl. Electromagn. Mech.* **2010**, *33*, 1231–1236. [[CrossRef](#)]
32. Wu, J.; Sun, Y.; Kang, Y.; Yang, Y. Theoretical Analyses of MFL Signal Affected by Discontinuity Orientation and Sensor-Scanning Direction. *IEEE Trans. Magn.* **2015**, *51*, 1–7. [[CrossRef](#)]
33. Azizzadeh, T.; Safizadeh, M.S. Investigation of the Lift-off Effect on the Corrosion Detection Sensitivity of Three-Axis MFL Technique. *J. Magn.* **2018**, *23*, 152–159. [[CrossRef](#)]
34. Wang, X.; Wu, X.; Xu, J.; Ba, H. Study on the Lift-off Effect on MFL Signals with Magnetic Circuit Model and 3D FEM. *Insight Non-Destr. Test. Cond. Monit.* **2012**, *54*, 505–510. [[CrossRef](#)]
35. Lunin, V.; Alexeevsky, D. Numerical Prediction of Signal for Magnetic Flux Leakage Benchmark Task. In Proceedings of the Review of Quantitative Nondestructive Evaluation, Green Bay, WI, USA, 27 July–1 August 2003; Volume 22, pp. 1830–1836.
36. Jia, Y.; Lu, Y.; Xiong, L.; Zhang, Y.; Wang, P.; Zhou, H. A Filtering Method for Suppressing the Lift-Off Interference in Magnetic Flux Leakage Detection of Rail Head Surface Defect. *Appl. Sci.* **2022**, *12*, 1740. [[CrossRef](#)]
37. Wu, J.; Fang, H.; Li, L.; Wang, J.; Huang, X.; Kang, Y.; Sun, Y.; Tang, C. A Lift-off-Tolerant Magnetic Flux Leakage Testing Method for Drill Pipes at Wellhead. *Sensors* **2017**, *17*, 201. [[CrossRef](#)]
38. Peng, L.; Huang, S.; Wang, S.; Zhao, W. A Simplified Lift-Off Correction for Three Components of the Magnetic Flux Leakage Signal for Defect Detection. *IEEE Trans. Instrum. Meas.* **2021**, *70*, 6005109. [[CrossRef](#)]
39. Wang, J.; Li, E.; Wu, J.; Xu, X. Linearization of the Lift-off Effect for Magnetic Flux Leakage Based on Fourier Transform. *Meas. Sci. Technol.* **2021**, *32*, 065012. [[CrossRef](#)]
40. Altschuler, E.; Pignotti, A. Nonlinear Model of Flaw Detection in Steel Pipes by Magnetic Flux Leakage. *NDT E Int.* **1995**, *28*, 35–40. [[CrossRef](#)]
41. Singh, W.S.; Rao, B.P.C.; Vaidyanathan, S.; Jayakumar, T.; Raj, B. Detection of Leakage Magnetic Flux from Near-Side and Far-Side Defects in Carbon Steel Plates Using a Giant Magneto-Resistive Sensor. *Meas. Sci. Technol.* **2008**, *19*, 015702. [[CrossRef](#)]
42. Sun, Y.; Feng, B.; Ye, Z.; Liu, S.; Li, D.; Kang, Y.; Gu, M.; Liu, C. Change Trends of Magnetic Flux Leakage with Increasing Magnetic Excitation. *Insight Non-Destr. Test. Cond. Monit.* **2015**, *57*, 689–696. [[CrossRef](#)]
43. Sun, Y.; Kang, Y. Magnetic Compression Effect in Present MFL Testing Sensor. *Sens. Actuators A Phys.* **2010**, *160*, 54–59. [[CrossRef](#)]
44. Sun, Y.; Kang, Y. A New MFL Principle and Method Based on Near-Zero Background Magnetic Field. *NDT E Int.* **2010**, *43*, 348–353. [[CrossRef](#)]
45. Katoh, M.; Nishio, K.; Yamaguchi, T. The Influence of Modeled B-H Curve on the Density of the Magnetic Leakage Flux Due to a Flaw Using Yoke-Magnetization. *NDT E Int.* **2004**, *37*, 603–609. [[CrossRef](#)]

46. Park, G.S.; Park, S.H. Analysis of the Velocity-Induced Eddy Current in MFL Type NDT. *IEEE Trans. Magn.* **2004**, *40*, 663–666. [[CrossRef](#)]
47. Gan, Z.; Chai, X. Numerical Simulation on Magnetic Flux Leakage Testing of the Steel Cable at Different Speed Title. In Proceedings of the 2011 International Conference on Electronics and Optoelectronics, Dalian, China, 29–31 July 2011; Volume 3, pp. 316–319. [[CrossRef](#)]
48. Li, Y.; Tian, G.Y.; Ward, S. Numerical Simulation on Magnetic Flux Leakage Evaluation at High Speed. *NDT E Int.* **2006**, *39*, 367–373. [[CrossRef](#)]
49. Antipov, A.G.; Markov, A.A. 3D Simulation and Experiment on High Speed Rail MFL Inspection. *NDT E Int.* **2018**, *98*, 177–185. [[CrossRef](#)]
50. Shin, Y. Numerical Prediction of Operating Conditions for Magnetic Flux Leakage Inspection of Moving Steel Sheets. *IEEE Trans. Magn.* **1997**, *33*, 2127–2130. [[CrossRef](#)]
51. Feng, B.; Deng, K.; Wang, S.; Chen, S.; Kang, Y. Theoretical Analysis on the Distribution of Eddy Current in Motion-Induced Eddy Current Testing and High-Speed MFL Testing. *J. Nondestruct. Eval.* **2022**, *41*, 59. [[CrossRef](#)]
52. Du, Z.; Ruan, J.; Peng, Y.; Yu, S.; Zhang, Y.; Gan, Y.; Li, T. 3-D FEM Simulation of Velocity Effects on Magnetic Flux Leakage Testing Signals. *IEEE Trans. Magn.* **2008**, *44*, 1642–1645. [[CrossRef](#)]
53. Wu, J.; Kang, Y.; Tu, J.; Sun, Y. Analysis of the Eddy-Current Effect in the Hi-Speed Axial MFL Testing for Steel Pipe. *Int. J. Appl. Electromagn. Mech.* **2014**, *45*, 193–199. [[CrossRef](#)]
54. Wu, J.; Fang, H.; Wang, J.; Kang, Y. Sensitivity Difference Caused by Eddy-Current Magnetic Field in Hi-Speed MFL Testing and Its Elimination Method. *Int. J. Appl. Electromagn. Mech.* **2016**, *52*, 1007–1014. [[CrossRef](#)]
55. Wu, J.; Xia, H.; Feng, B.; Li, E.; Huang, X.; Kang, Y. The Effect of Motion-Induced Eddy Current on Axial MFL Inspection for a Steel Pipe. *Int. J. Appl. Electromagn. Mech.* **2019**, *59*, 1187–1193. [[CrossRef](#)]
56. Feng, B.; Kang, Y.; Sun, Y.; Yang, Y.; Yan, X. Influence of Motion Induced Eddy Current on the Magnetization of Steel Pipe and MFL Signal. *Int. J. Appl. Electromagn. Mech.* **2016**, *52*, 357–362. [[CrossRef](#)]
57. Wu, J.; Xia, H.; Feng, B.; Li, E.; Huang, X.; Kang, Y. The Effect of Motion-Induced Eddy Current on Circumferential Magnetization in MFL Testing for a Steel Pipe. *IEEE Trans. Magn.* **2017**, *53*, 6201506. [[CrossRef](#)]
58. Katragadda, G.; Lord, W.; Sun, Y.S.; Udpa, S.; Udpa, L. Alternative Magnetic Flux Leakage Modalities for Pipeline Inspection. *IEEE Trans. Magn.* **1996**, *32*, 1581–1584. [[CrossRef](#)]
59. Piao, G.; Li, J.; Udpa, L.; Udpa, S.; Deng, Y. The Effect of Motion-Induced Eddy Currents on Three-Axis MFL Signals for High-Speed Rail Inspection. *IEEE Trans. Magn.* **2021**, *57*, 6200211. [[CrossRef](#)]
60. Piao, G.; Guo, J.; Hu, T.; Leung, H. The Effect of Motion-Induced Eddy Current on High-Speed Magnetic Flux Leakage (MFL) Inspection for Thick-Wall Steel Pipe. *Res. Nondestruct. Eval.* **2020**, *31*, 48–67. [[CrossRef](#)]
61. Wang, P.; Gao, Y.; Tian, G.; Wang, H. Velocity Effect Analysis of Dynamic Magnetization in High Speed Magnetic Flux Leakage Inspection. *NDT E Int.* **2014**, *64*, 7–12. [[CrossRef](#)]
62. Pullen, A.L.; Charlton, P.C.; Pearson, N.R.; Whitehead, N.J. Practical Evaluation of Velocity Effects on the Magnetic Flux Leakage Technique for Storage Tank Inspection. *Insight* **2020**, *62*, 73–80. [[CrossRef](#)]
63. Pullen, A.L.; Charlton, P.C.; Pearson, N.R.; Whitehead, N.J. Magnetic Flux Leakage Scanning Velocities for Tank Floor Inspection. *IEEE Trans. Magn.* **2018**, *54*, 1–8. [[CrossRef](#)]
64. Zhang, L.; Belblidia, F.; Cameron, I.; Sienz, J.; Boat, M.; Pearson, N. Influence of Specimen Velocity on the Leakage Signal in Magnetic Flux Leakage Type Nondestructive Testing. *J. Nondestruct. Eval.* **2015**, *34*, 6. [[CrossRef](#)]
65. Usarek, Z.; Chmielewski, M.; Piotrowski, L. Reduction of the Velocity Impact on the Magnetic Flux Leakage Signal. *J. Nondestruct. Eval.* **2019**, *38*, 28. [[CrossRef](#)]
66. Antipov, A.G.; Markov, A.A. Using a Tail Field in High-Speed Magnetic Flux Leakage Testing. *J. Nondestruct. Eval.* **2022**, *41*, 1–9. [[CrossRef](#)]
67. Feng, B.; Kang, Y.; Sun, Y. Theoretical Analysis and Numerical Simulation of the Feasibility of Inspecting Nonferromagnetic Conductors by an MFL Testing Apparatus. *Res. Nondestruct. Eval.* **2016**, *27*, 100–111. [[CrossRef](#)]
68. Feng, B.; Ribeiro, A.L.; Rocha, T.J.; Ramos, H.G. Comparison of Inspecting Non-Ferromagnetic and Ferromagnetic Metals Using Velocity Induced Eddy Current Probe. *Sensors* **2018**, *18*, 3199. [[CrossRef](#)]
69. Rocha, T.J.; Ramos, H.G.; Lopes Ribeiro, A.; Pasadas, D.J. Magnetic Sensors Assessment in Velocity Induced Eddy Current Testing. *Sens. Actuators A Phys.* **2015**, *228*, 55–61. [[CrossRef](#)]
70. Rocha, T.J.; Ramos, H.G.; Lopes Ribeiro, A.; Pasadas, D.J.; Angani, C.S. Studies to Optimize the Probe Response for Velocity Induced Eddy Current Testing in Aluminium. *Measurement* **2015**, *67*, 108–115. [[CrossRef](#)]
71. Rocha, T.J.; Ramos, H.G.; Ribeiro, A.L.; Pasadas, D.J. Evaluation of Subsurface Defects Using Diffusion of Motion-Induced Eddy Currents. *IEEE Trans. Instrum. Meas.* **2016**, *65*, 1182–1187. [[CrossRef](#)]
72. Yuan, F.; Yu, Y.; Li, L.; Tian, G. Investigation of DC Electromagnetic-Based Motion Induced Eddy Current on NDT for Crack Detection. *IEEE Sens. J.* **2021**, *21*, 7449–7457. [[CrossRef](#)]
73. Uhlig, R.P.; Zec, M.; Brauer, H.; Thess, A. Lorentz Force Eddy Current Testing: A Prototype Model. *J. Nondestruct. Eval.* **2012**, *31*, 357–372. [[CrossRef](#)]
74. Dölker, E.M.; Schmidt, R.; Gorges, S.; Otterbach, J.M.; Petković, B.; Strohmeier, D.; Eichardt, R.; Brauer, H.; Hauelsen, J. Elastic Net Regularization in Lorentz Force Evaluation. *NDT E Int.* **2018**, *99*, 141–154. [[CrossRef](#)]

75. Mengelkamp, J.; Carlstedt, M.; Weise, K.; Ziolkowski, M.; Brauer, H.; Haueisen, J. Current Density Reconstructions for Lorentz Force Evaluation. *Res. Nondestruct. Eval.* **2017**, *28*, 76–100. [[CrossRef](#)]
76. Weise, K.; Schmidt, R.; Carlstedt, M.; Ziolkowski, M.; Brauer, H.; Toepfer, H. Optimal Magnet Design for Lorentz Force Eddy-Current Testing. *IEEE Trans. Magn.* **2015**, *51*, 1–15. [[CrossRef](#)]
77. Carlstedt, M.; Porzig, K.; Uhlig, R.P.; Zec, M.; Ziolkowski, M.; Brauer, H. Application of Lorentz Force Eddy Current Testing and Eddy Current Testing on Moving Nonmagnetic Conductors. *Int. J. Appl. Electromagn. Mech.* **2014**, *45*, 519–526. [[CrossRef](#)]
78. Kasai, N.; Sekine, K.; Maruyama, H. Influence of Corrosion Products on Magnetic Flux Leakage Signals in Inspection of Far-Side Metal-Loss Defects in Oil Storage Tank Bottom Floors. *J. Japan Pet. Inst.* **2004**, *47*, 19–26. [[CrossRef](#)]
79. Long, Y.; Huang, S.; Peng, L.; Wang, S.; Zhao, W. A Novel Compensation Method of Probe Gesture for Magnetic Flux Leakage Testing. *IEEE Sens. J.* **2021**, *21*, 10854–10863. [[CrossRef](#)]
80. Wang, Y.; Melikhov, Y.; Meydan, T.; Yang, Z.; Wu, D.; Wu, B.; He, C.; Liu, X. Stress-Dependent Magnetic Flux Leakage: Finite Element Modelling Simulations Versus Experiments. *J. Nondestruct. Eval.* **2020**, *39*, 1–9. [[CrossRef](#)]
81. Mandal, K.; Corey, A.; Loukas, M.E.; Weyman, P.; Eichenberger, J.; Atherton, D.L. The Effects of Defect Depth and Bending Stress on Magnetic Barkhausen Noise and Flux-Leakage Signals. *J. Phys. D Appl. Phys.* **1997**, *30*, 1976–1983. [[CrossRef](#)]
82. Wang, Y.; Liu, X.; Wu, B.; Xiao, J.; Wu, D.; He, C. Dipole Modeling of Stress-Dependent Magnetic Flux Leakage. *NDT E Int.* **2018**, *95*, 1–8. [[CrossRef](#)]
83. Gao, G.; Lian, M.; Xu, Y.; Qin, Y.; Gao, L. The Effect of Variable Tensile Stress on the MFL Signal Response of Defective Wire Ropes. *Insight Non-Destr. Test. Cond. Monit.* **2016**, *58*, 135–141. [[CrossRef](#)]
84. Shi, P.; Bai, P.; Chen, H.E.; Su, S.; Chen, Z. The Magneto-Elastoplastic Coupling Effect on the Magnetic Flux Leakage Signal. *J. Magn. Magn. Mater.* **2020**, *504*, 166669. [[CrossRef](#)]
85. Ryu, K.S.; Atherton, D.L.; Clapham, L. Effect of Pit Geometry and Bulk Stress on Near- and Far-Side Calculated MFL Signals. *J. Phys. D Appl. Phys.* **2002**, *35*, 2693–2697. [[CrossRef](#)]
86. Xiao-Meng, L.; Hong-Sheng, D.; Shi-Wu, B. Research on the Stress-Magnetism Effect of Ferromagnetic Materials Based on Three-Dimensional Magnetic Flux Leakage Testing. *NDT E Int.* **2014**, *62*, 50–54. [[CrossRef](#)]
87. Van Der Horst, M.P.; Van Kreveld, S.L.; Kaminski, M.L. Effect of Stress-Induced Magnetization on Crack Monitoring by Self Magnetic Flux Leakage Method. *Int. J. Appl. Electromagn. Mech.* **2019**, *60*, 113–130. [[CrossRef](#)]
88. Wu, L.; Yao, K.; Shi, P.; Zhao, B.; Wang, Y.S. Influence of Inhomogeneous Stress on Biaxial 3D Magnetic Flux Leakage Signals. *NDT E Int.* **2020**, *109*, 102178. [[CrossRef](#)]
89. Babbar, V.; Bryne, J.; Clapham, L. Mechanical Damage Detection Using Magnetic Flux Leakage Tools: Modeling the Effect of Dent Geometry and Stresses. *NDT E Int.* **2005**, *38*, 471–477. [[CrossRef](#)]
90. Kashafi, M.; Clapham, L.; Krause, T.W.; Underhill, P.R.; Krause, A.K. Stress-Induced Self-Magnetic Flux Leakage at Stress Concentration Zone. *IEEE Trans. Magn.* **2021**, *57*, 1–8. [[CrossRef](#)]
91. Babbar, V.; Shiari, B.; Clapham, L. Mechanical Damage Detection With Magnetic Flux Leakage Tools: Modeling the Effect of Localized Residual Stresses. *IEEE Trans. Magn.* **2004**, *40*, 43–49. [[CrossRef](#)]
92. Deng, Z.; Sun, Y.; Yang, Y.; Kang, Y. Effects of Surface Roughness on Magnetic Flux Leakage Testing of Micro-Cracks. *Meas. Sci. Technol.* **2017**, *28*, 045003. [[CrossRef](#)]
93. Yang, Y.; Li, L.; Deng, Z.; Kang, Y. Theoretical Analysis and Simulation of a New SNR Improvement Method for the Rough Surface Crack in MFL Detection. *Int. J. Appl. Electromagn. Mech.* **2016**, *52*, 1401–1408. [[CrossRef](#)]
94. Rao, B.P.C.; Thirunavukkarasu, S.; Nand, K.K.; Jayakumar, T.; Kalyanasundaram, P.; Raj, B. Enhancement of Magnetic Flux Leakage Images of Defects in Carbon Steel Using Eigen Vector Based Approach. *Nondestruct. Test. Eval.* **2008**, *23*, 35–42. [[CrossRef](#)]
95. Li, E.; Wang, J.; Wu, J.; Kang, Y. Spatial-Spectrum-Based Measurement of the Surface Roughness of Ferromagnetic Components Using Magnetic Flux Leakage Method. *IEEE Trans. Instrum. Meas.* **2021**, *70*, 1–10. [[CrossRef](#)]
96. Labinac, V.; Erceg, N.; Kotnik-Karuza, D. Magnetic Field of a Cylindrical Coil. *Am. J. Phys.* **2006**, *74*, 621–627. [[CrossRef](#)]
97. Wang, J.; She, S.; Zhang, S. An Improved Helmholtz Coil and Analysis of Its Magnetic Field Homogeneity. *Rev. Sci. Instrum.* **2002**, *73*, 2175. [[CrossRef](#)]
98. Sun, Y.; Kang, Y. An Opening Electromagnetic Transducer. *J. Appl. Phys.* **2013**, *114*, 214904. [[CrossRef](#)]
99. Sun, Y.; Wu, J.; Feng, B.; Kang, Y. An Opening Electric-MFL Detector for the NDT of In-Service Mine Hoist Wire. *IEEE Sens. J.* **2014**, *14*, 2042–2047.
100. Wang, S.; Feng, B.; Tang, J.; Chen, Y.; Kang, Y. A Novel AC-MFL Probe Based on the Parallel Cables Magnetizing Technique. *J. Nondestruct. Eval.* **2022**, *41*, 1–8. [[CrossRef](#)]
101. Chang, Y.; Jiao, J.; Li, G.; Liu, X.; He, C.; Wu, B. Effects of Excitation System on the Performance of Magnetic-Flux-Leakage-Type Non-Destructive Testing. *Sens. Actuators A Phys.* **2017**, *268*, 201–212. [[CrossRef](#)]
102. Parra-Raad, J.A.; Roa-Prada, S. Multi-Objective Optimization of a Magnetic Circuit for Magnetic Flux Leakage-Type Non-Destructive Testing. *J. Nondestruct. Eval.* **2016**, *35*, 1–12. [[CrossRef](#)]
103. Chen, G.; Li, W.; Wang, Z. Structural Optimization of 2-D Array Probe for Alternating Current Field Measurement. *NDT E Int.* **2007**, *40*, 455–461. [[CrossRef](#)]
104. Gotoh, Y.; Takahashi, N. 3-D Nonlinear Eddy-Current Analysis of Alternating Magnetic Flux Leakage Testing—Analysis of One Crack and Two Cracks. *IEEE Trans. Magn.* **2002**, *38*, 1209–1212. [[CrossRef](#)]

105. Gotoh, Y.; Takahashi, N. Study on Problems in Detecting Plural Cracks by Alternating Flux Leakage Testing Using 3-D Nonlinear Eddy Current Analysis. *IEEE Trans. Magn.* **2003**, *39*, 1527–1530. [[CrossRef](#)]
106. Gotoh, Y.; Takahashi, N. Proposal of Detecting Method of Outer Side Crack by Alternating Flux Leakage Testing Using 3-D Nonlinear FEM. *IEEE Trans. Magn.* **2006**, *42*, 1415–1418. [[CrossRef](#)]
107. Gotoh, Y.; Takahashi, N. Three-Dimensional FEM Analysis of Electromagnetic Inspection of Outer Side Defects on Steel Tube Using Inner Coil. *IEEE Trans. Magn.* **2007**, *43*, 1733. [[CrossRef](#)]
108. Hayashi, M.; Kawakami, T.; Saito, T.; Sakai, K.; Kiwa, T.; Tsukada, K. Imaging of Defect Signal of Reinforcing Steel Bar at High Lift-Off Using a Magnetic Sensor Array by Unsaturated AC Magnetic Flux Leakage Testing. *IEEE Trans. Magn.* **2021**, *57*, 2020–2023. [[CrossRef](#)]
109. Sophian, A.; Tian, G.Y.; Zairi, S. Pulsed Magnetic Flux Leakage Techniques for Crack Detection and Characterisation. *Sens. Actuators A Phys.* **2006**, *125*, 186–191. [[CrossRef](#)]
110. Wilson, J.W.; Tian, G.Y. Pulsed Electromagnetic Methods for Defect Detection and Characterisation. *NDT E Int.* **2007**, *40*, 275–283. [[CrossRef](#)]
111. Wilson, J.W.; Kaba, M.; Tian, G.Y.; Licciardi, S. Feature Extraction and Integration for the Quantification of PMFL Data. *Nondestruct. Test. Eval.* **2010**, *25*, 101–109. [[CrossRef](#)]
112. Wang, P.; Xiong, L.; Sun, Y.; Wang, H.; Tian, G. Features Extraction of Sensor Array Based PMFL Technology for Detection of Rail Cracks. *Measurement* **2014**, *47*, 613–626. [[CrossRef](#)]
113. Tang, Y.; Pan, M.C.; Luo, F.L.; Tan, X.L. Experimental and Finite Element Analysis Study of 3D Magnetic Field Sensing for Pulsed Magnetic Flux Leakage Defect Characterization. *Insight* **2011**, *53*, 497–506. [[CrossRef](#)]
114. Ying, T.; Meng, P.; Feilu, C. Feature Extraction Based on the Principal Component Analysis for Pulsed Magnetic Flux Leakage Testing. In Proceedings of the 2011 International Conference on Mechatronic Science, Electric Engineering and Computer, MEC, Jilin, China, 19–22 August 2011; pp. 2563–2566.
115. Wu, D.; Liu, Z.; Wang, X.; Su, L. Composite Magnetic Flux Leakage Detection Method for Pipelines Using Alternating Magnetic Field Excitation. *NDT E Int.* **2017**, *91*, 148–155. [[CrossRef](#)]
116. Wang, R.; Kang, Y.; Tang, J.; Feng, B.; Deng, Y. A Novel Magnetic Flux Leakage Testing Method Based on AC and DC Composite Magnetization. *J. Nondestruct. Eval.* **2020**, *39*, 1–11. [[CrossRef](#)]
117. Gotoh, Y.; Takahashi, N. Evaluation of Detecting Method with AC and DC Excitations of Opposite-Side Defect in Steel Using 3-D Nonlinear FEM Taking the Minor Loop into Account. *IEEE Trans. Magn.* **2008**, *44*, 1622–1625. [[CrossRef](#)]
118. Singh, W.S.; Rao, B.P.C.; Thirunavukkarasu, S.; Jayakumar, T. Flexible GMR Sensor Array for Magnetic Flux Leakage Testing of Steel Track Ropes. *J. Sens.* **2012**, *2012*, 1–6. [[CrossRef](#)]
119. Kataoka, Y.; Murayama, S.; Wakiwaka, H.; Shinoura, O. Application of GMR Line Sensor to Detect the Magnetic Flux Distribution for Nondestructive Testing. *Int. J. Appl. Electromagn. Mech.* **2001**, *15*, 47–52. [[CrossRef](#)]
120. Tehranchi, M.M.; Ranjbaran, M.; Eftekhari, H. Double Core Giant Magneto-Impedance Sensors for the Inspection of Magnetic Flux Leakage from Metal Surface Cracks. *Sens. Actuators A Phys.* **2011**, *170*, 55–61. [[CrossRef](#)]
121. Jin, Z.; Mohd Noor Sam, M.A.I.; Oogane, M.; Ando, Y. Serial MTJ-Based TMR Sensors in Bridge Configuration for Detection of Fractured Steel Bar in Magnetic Flux Leakage Testing. *Sensors* **2021**, *21*, 668. [[CrossRef](#)]
122. Kallias, G.; Devlin, E.; Christides, C.; Niarchos, D. High Tc SQUID Sensor System for Non-Destructive Evaluation. *Sens. Actuators A Phys.* **2000**, *85*, 239–243. [[CrossRef](#)]
123. Krause, H.J.; Kreutzbruck, M.V. Recent Developments in SQUID NDE. *Phys. C Supercond. Its Appl.* **2002**, *368*, 70–79. [[CrossRef](#)]
124. Park, G.S.; Park, E.S. Improvement of the Sensor System in Magnetic Flux Leakage-Type Nondestructive Testing (NDT). *IEEE Trans. Magn.* **2002**, *38*, 1277–1280. [[CrossRef](#)]
125. Jia, Y.; Liang, K.; Wang, P.; Ji, K.; Xu, P. Enhancement Method of Magnetic Flux Leakage Signals for Rail Track Surface Defect Detection. *IET Sci. Meas. Technol.* **2020**, *14*, 711–717. [[CrossRef](#)]
126. Wu, J.; Yang, Y.; Li, E.; Deng, Z.; Kang, Y.; Tang, C.; Sunny, A.I. A High-Sensitivity MFL Method for Tiny Cracks in Bearing Rings. *IEEE Trans. Magn.* **2018**, *54*, 6201308. [[CrossRef](#)]
127. Tang, J.; Wang, R.; Zhang, J.; Kang, Y. The Influence of Magnetic Head's Pose on Magnetic Flux Leakage Detection. *Int. J. Appl. Electromagn. Mech.* **2020**, *64*, 493–500. [[CrossRef](#)]
128. Li, E.; Kang, Y.; Tang, J.; Wu, J. A New Micro Magnetic Bridge Probe in Magnetic Flux Leakage for Detecting Micro-Cracks. *J. Nondestruct. Eval.* **2018**, *37*, 1–9. [[CrossRef](#)]
129. Li, E.; Chen, X.; Wu, J.; Zhu, J.; Kang, Y. A Spatial Broadband Magnetic Flux Leakage Method for Trans-Scale Defect Detection. *J. Nondestruct. Eval.* **2022**, *41*, 1–12. [[CrossRef](#)]
130. Liu, S.; Sun, Y.; He, L.; Kang, Y. Magnetic Focusing Method and Sensor in Surface Topography Testing for Ferromagnetic Materials. *Sens. Actuators A Phys.* **2019**, *285*, 531–542. [[CrossRef](#)]
131. Dehui, W.; Lingxin, S.; Xiaohong, W.; Zhitian, L. A Novel Non-Destructive Testing Method by Measuring the Change Rate of Magnetic Flux Leakage. *J. Nondestruct. Eval.* **2017**, *36*, 1–11. [[CrossRef](#)]
132. Tang, J.; Wang, R.; Liu, B.; Kang, Y. A Novel Magnetic Flux Leakage Method Based on the Ferromagnetic Lift-off Layer with through Groove. *Sens. Actuators A Phys.* **2021**, *332*, 113091. [[CrossRef](#)]
133. Nara, T.; Takanashi, Y.; Mizuide, M. A Sensor Measuring the Fourier Coefficients of the Magnetic Flux Density for Pipe Crack Detection Using the Magnetic Flux Leakage Method. *J. Appl. Phys.* **2011**, *109*, 07E305. [[CrossRef](#)]

134. Philip, J.; Rao, C.B.; Jayakumar, T.; Raj, B. New Optical Technique for Detection of Defects in Ferromagnetic Materials and Components. *NDT E Int.* **2000**, *33*, 289–295. [[CrossRef](#)]
135. Mahendran, V.; Philip, J. Nanofluid Based Optical Sensor for Rapid Visual Inspection of Defects in Ferromagnetic Materials. *Appl. Phys. Lett.* **2012**, *100*, 1–4. [[CrossRef](#)]
136. Mahendran, V.; Philip, J. Naked Eye Visualization of Defects in Ferromagnetic Materials and Components. *NDT E Int.* **2013**, *60*, 100–109. [[CrossRef](#)]
137. Lee, J.; Wang, R.; Shoji, T.; Hong, S. Non-Destructive Testing in the High-Temperature Regime by Using a Magneto-Optical Film. *NDT E Int.* **2008**, *41*, 420–426. [[CrossRef](#)]
138. Tehranchi, M.M.; Hamidi, S.M.; Eftekhari, H.; Karbaschi, M.; Ranjbaran, M. The Inspection of Magnetic Flux Leakage from Metal Surface Cracks by Magneto-Optical Sensors. *Sens. Actuators A Phys.* **2011**, *172*, 365–368. [[CrossRef](#)]
139. Carvalho, A.A.; Rebello, J.M.A.; Sagrilo, L.V.S.; Camerini, C.S.; Miranda, I.V.J. MFL Signals and Artificial Neural Networks Applied to Detection and Classification of Pipe Weld Defects. *NDT E Int.* **2006**, *39*, 661–667. [[CrossRef](#)]
140. Hwang, K.; Mandayam, S.; Udpa, S.S.; Udpa, L.; Lord, W.; Atzal, M. Characterization of Gas Pipeline Inspection Signals Using Wavelet Basis Function Neural Networks. *NDT E Int.* **2000**, *33*, 531–545. [[CrossRef](#)]
141. Khodayari-Rostamabad, A.; Reilly, J.P.; Nikolova, N.K.; Hare, J.R.; Pasha, S. Machine Learning Techniques for the Analysis of Magnetic Flux Leakage Images in Pipeline Inspection. *IEEE Trans. Magn.* **2009**, *45*, 3073–3084. [[CrossRef](#)]
142. Kandroodi, M.R.; Araabi, B.N.; Bassiri, M.M.; Ahmadabadi, M.N. Estimation of Depth and Length of Defects from Magnetic Flux Leakage Measurements: Verification with Simulations, Experiments, and Pigging Data. *IEEE Trans. Magn.* **2017**, *53*, 1–10. [[CrossRef](#)]
143. Feng, J.; Li, F.; Lu, S.; Liu, J.; Ma, D. Injurious or Noninjurious Defect Identification from MFL Images in Pipeline Inspection Using Convolutional Neural Network. *IEEE Trans. Instrum. Meas.* **2017**, *66*, 1883–1892. [[CrossRef](#)]
144. Lu, S.; Feng, J.; Zhang, H.; Liu, J.; Wu, Z. An Estimation Method of Defect Size from MFL Image Using Visual Transformation Convolutional Neural Network. *IEEE Trans. Ind. Inform.* **2019**, *15*, 213–224. [[CrossRef](#)]
145. Wu, Z.; Deng, Y.; Liu, J.; Wang, L. A Reinforcement Learning-Based Reconstruction Method for Complex Defect Profiles in MFL Inspection. *IEEE Trans. Instrum. Meas.* **2021**, *70*, 1–10. [[CrossRef](#)]
146. Sun, H.; Peng, L.; Huang, S.; Li, S.; Long, Y.; Wang, S.; Zhao, W. Development of a Physics-Informed Doubly Fed Cross-Residual Deep Neural Network for High-Precision Magnetic Flux Leakage Defect Size Estimation. *IEEE Trans. Ind. Inform.* **2022**, *18*, 1629–1640. [[CrossRef](#)]
147. Yan, M.; Udpa, S.; Mandayam, S.; Sun, Y.; Sacks, P.; Lord, W. Solution of Inverse Problems in Electromagnetic NDE Using Finite Element Methods. *IEEE Trans. Magn.* **1998**, *34*, 2920–2923. [[CrossRef](#)]
148. Chen, Z.; Preda, G.; Mihalache, O.; Miya, K. Reconstruction of Crack Shapes from the MFLT Signals by Using a Rapid Forward Solver and an Optimization Approach. *IEEE Trans. Magn.* **2002**, *38*, 1025–1028. [[CrossRef](#)]
149. Ramuhalli, P.; Udpa, L.; Udpa, S.S. Neural Network-Based Inversion Algorithms in Magnetic Flux Leakage Nondestructive Evaluation. *J. Appl. Phys.* **2003**, *93*, 8274–8276. [[CrossRef](#)]
150. Amineh, R.K.; Koziel, S.; Nikolova, N.K.; Bandler, J.W.; Reilly, J.P. A Space Mapping Methodology for Defect Characterization from Magnetic Flux Leakage Measurements. *IEEE Trans. Magn.* **2008**, *44*, 2058–2065. [[CrossRef](#)]
151. Amineh, R.K.; Nikolova, N.K.; Reilly, J.P.; Hare, J.R. Characterization of Surface-Breaking Cracks Using One Tangential Component of Magnetic Leakage Field Measurements. *IEEE Trans. Magn.* **2008**, *44*, 516–524. [[CrossRef](#)]
152. Liu, X.; Deng, Y.; Zeng, Z.; Udpa, L.; Udpa, S.S. Model-Based Inversion Technique Using Element-Free Galerkin Method and State Space Search. *IEEE Trans. Magn.* **2009**, *45*, 1486–1489. [[CrossRef](#)]
153. Priewald, R.H.; Magele, C.; Ledger, P.D.; Pearson, N.R.; Mason, J.S.D. Fast Magnetic Flux Leakage Signal Inversion for the Reconstruction of Arbitrary Defect Profiles in Steel Using Finite Elements. *IEEE Trans. Magn.* **2013**, *49*, 506–516. [[CrossRef](#)]
154. Chen, J.; Huang, S.; Zhao, W. Three-Dimensional Defect Inversion from Magnetic Flux Leakage Signals Using Iterative Neural Network. *IET Sci. Meas. Technol.* **2015**, *9*, 418–426. [[CrossRef](#)]
155. Feng, J.; Li, F.; Lu, S.; Liu, J. Fast Reconstruction of Defect Profiles from Magnetic Flux Leakage Measurements Using a RBFNN Based Error Adjustment Methodology. *IET Sci. Meas. Technol.* **2017**, *11*, 262–269. [[CrossRef](#)]
156. Li, F.; Feng, J.; Zhang, H.; Liu, J.; Lu, S.; Ma, D. Quick Reconstruction of Arbitrary Pipeline Defect Profiles from MFL Measurements Employing Modified Harmony Search Algorithm. *IEEE Trans. Instrum. Meas.* **2018**, *67*, 2200–2213. [[CrossRef](#)]
157. Yu, G.; Liu, J.; Zhang, H.; Liu, C. An Iterative Stacking Method for Pipeline Defect Inversion with Complex MFL Signals. *IEEE Trans. Instrum. Meas.* **2020**, *69*, 3780–3788. [[CrossRef](#)]
158. Wu, Z.; Deng, Y.; Wang, L. A Pinning Actor-Critic Structure-Based Algorithm for Sizing Complex-Shaped Depth Profiles in MFL Inspection with High Degree of Freedom. *Complexity* **2021**, *2021*, 1–12. [[CrossRef](#)]
159. Zhang, H.; Wang, L.; Wang, J.; Zuo, F.; Wang, J.; Liu, J. A Pipeline Defect Inversion Method with Erratic MFL Signals Based on Cascading Abstract Features. *IEEE Trans. Instrum. Meas.* **2022**, *71*, 3506711. [[CrossRef](#)]
160. Ramuhalli, P.; Udpa, L.; Udpa, S.S. Electromagnetic NDE Signal Inversion by Function-Approximation Neural Networks. *IEEE Trans. Magn.* **2002**, *38*, 3633–3642. [[CrossRef](#)]
161. Xu, C.; Wang, C.; Ji, F.; Yuan, X. Finite-Element Neural Network-Based Solving 3-D Differential Equations in Mfl. *IEEE Trans. Magn.* **2012**, *48*, 4747–4756. [[CrossRef](#)]

162. Hari, K.C.; Nabi, M.; Kulkarni, S.V. Improved FEM model for defect-shape construction from MFL signal by using genetic algorithm. *IET Sci. Meas. Technol.* **2007**, *14*, 196–200. [[CrossRef](#)]
163. Han, W.; Wu, Z.; Zhou, M.; Hou, E.; Su, X.; Wang, P.; Tian, G. Magnetic Flux Leakage Signal Inversion Based on Improved Efficient Population Utilization Strategy for Particle Swarm Optimization. *Russ. J. Nondestruct. Test.* **2017**, *53*, 862–873. [[CrossRef](#)]
164. Han, W.; Xu, J.; Wang, P.; Tian, G. Defect Profile Estimation from Magnetic Flux Leakage Signal via Efficient Managing Particle Swarm Optimization. *Sensors* **2014**, *14*, 10361–10380. [[CrossRef](#)]
165. Zhang, Y.; Ye, Z.; Wang, C. A Fast Method for Rectangular Crack Sizes Reconstruction in Magnetic Flux Leakage Testing. *NDT E Int.* **2009**, *42*, 369–375. [[CrossRef](#)]
166. Han, W.; Xu, J.; Zhou, M.; Tian, G.; Wang, P.; Shen, X.; Hou, E. Cuckoo Search and Particle Filter-Based Inversing Approach to Estimating Defects via Magnetic Flux Leakage Signals. *IEEE Trans. Magn.* **2016**, *52*, 1–11. [[CrossRef](#)]
167. Zhang, D.; Huang, C.; Fei, J. Defect Reconstruction from Magnetic Flux Leakage Measurements Employing Modified Cuckoo Search Algorithm. *Math. Biosci. Eng.* **2021**, *18*, 1898–1925. [[CrossRef](#)] [[PubMed](#)]
168. Vértesy, G.; Gasparics, A.; Tomáš, I. Inspection of Local Wall Thinning by Different Magnetic Methods. *J. Nondestruct. Eval.* **2018**, *37*, 1–8. [[CrossRef](#)]
169. Deng, Z.; Li, T.; Zhang, J.; Song, X.; Kang, Y. A Magnetic Permeability Perturbation Testing Methodology and Experimental Research for Deeply Buried Defect in Ferromagnetic Materials. *NDT E Int.* **2022**, *131*, 102694. [[CrossRef](#)]
170. Sun, Y.; Kang, Y.; Qiu, C. A New NDT Method Based on Permanent Magnetic Field Perturbation. *NDT E Int.* **2011**, *44*, 1–7. [[CrossRef](#)]
171. Sun, Y.; Kang, Y.; Qiu, C. A Permanent Magnetic Perturbation Testing Sensor. *Sens. Actuators A Phys.* **2009**, *155*, 226–232. [[CrossRef](#)]